

39 **Exploring impacts of forest management strategies on water partitioning in a drought-sensitive catchment**
40 **using a tracer-aided ecohydrological framework**

41 Cong Jiang ¹, Doerthe Tetzlaff ^{1,2,3}, Songjun Wu¹, Christian Birkel ^{1,4}, Hjalmar Laudon ⁵, Chris Soulsby ^{1,3,5,6}

42 ¹ Leibniz-Institute of Freshwater Ecology and Inland Fisheries (IGB), Department of Ecohydrology and
43 Biogeochemistry, Berlin, Germany

44 ² Department of Geography, Humboldt University Berlin, Berlin, Germany

45 ³ Northern Rivers Institute, University of Aberdeen, Aberdeen, UK

46 ⁴ Department of Geography, University of Costa Rica, San Pedro, Costa Rica

47 ⁵ Department of Forest Ecology and Management, Swedish University of Agricultural Science (SLU), Sweden

48 ⁶ Chair of Water Resources Management and Modeling of Hydrosystems, Technical University Berlin, Berlin,
49 Germany

50 *Correspondence to:* Cong Jiang (cong.jiang@igb-berlin.de)

51 **Abstract.** Land use strongly influences water partitioning, water availability, and ecohydrological resilience in
52 drought-sensitive regions. Forest management plays a critical role through its effects on water use, which depends
53 on forest type, forest density, root water uptake, yet the ecohydrological consequences of different forest
54 management strategies—particularly in terms of blue and green water fluxes—remain poorly quantified. Here,
55 we develop and apply a parsimonious, tracer-aided forest management scenario framework using the conceptual
56 ecohydrological model EcoPlot-iso, designed to isolate the dominant vegetation-structural controls on long-term
57 water partitioning. We investigated how variations in generic forest type (e.g., broadleaf vs. conifer), forest density,
58 and root distribution influence water partitioning and ecohydrological resilience under different wetness
59 conditions in the drought-sensitive lowland Demnitzer Millcreek catchment (DMC), northeastern Germany.
60 Baseline simulations for the period 2000–2024 were conducted at three forest sites and used to develop forest-
61 type-specific reference conditions for comparison with alternative forest management scenarios. A key innovation
62 in this version of EcoPlot-iso was the integration of a depth-dependent root water uptake function, allowing
63 simulation of transpiration across soil layers under with-contrasting rooting distributions -corresponding to
64 different and-stand ages. The model was calibrated and validated using seven years of soil moisture and three
65 years of soil water isotope ($\delta^2\text{H}$) data through a multi-criteria approach. Results showed that, on average,
66 evapotranspiration was highest under conifers, exceeding broadleaf forests and agroforestry by 7% and 11%,
67 respectively, while agroforestry exhibited the greatest groundwater recharge. Significant differences in water
68 partitioning between dry and wet years were observed across management scenarios. ~~Comparisons between wet~~
69 ~~and dry years indicate that c~~Conifer forests showed ed the strongerst transpiration contrasts relative tohan broadleaf
70 forests in early spring, while the wet-dry-year contrast between the two forest types was largest while peak
71 ~~drought sensitivity occurs~~ in late spring. Our findings highlight the potential of agroforestry, such as crop-tree
72 mixtures, to mitigate drought impacts, on soil water availability and groundwater recharge. Overall, this study
73 demonstrates how a parsimonious, tracer-aided scenario framework can be used as a decision-support tool to
74 quantify and visualize the effects of land use change on water availability in data-limited regions, supporting more
75 informed decision-making and enhanced ecohydrological resilience under increasing drought pressure.

76

116 1 Introduction

117 Land use plays a crucial role in regulating water, carbon, energy, and nutrient cycles by mediating ecohydrological
118 fluxes and soil water storage dynamics which link interactions between the atmosphere, soils, vegetation and
119 biogeochemical processes (Mahmood et al., 2014; Pielke et al., 2011; Smith et al., 2021; Sterling et al., 2013).
120 Among the different types of land cover, forests are particularly important elements of the land use mosaic,
121 providing a range of ecosystem services, including enhancing infiltration, stabilizing soils, storing carbon,
122 supplying timber and fuelwood, as well as buffering extreme climate events (Bonan, 2008). However, there are
123 clear trade-offs, as forests and trees also tend to use more water than contrasting land uses (Bosch & Hewlett,
124 1982; Calder, 1998). This is because their high Leaf Area Index (LAI) and canopy storage capacities often result
125 in greater interception losses and canopy evaporation, while their deeper and denser rooting networks can sustain
126 transpiration when top soils dry out (Wang-Erlandsson et al., 2014). Consequently, forest management decisions,
127 (e.g., afforestation, thinning, ~~and forest type selection etc.~~) can significantly affect water yield ~~and~~, the partitioning
128 into blue water fluxes (runoff ~~and~~ groundwater recharge) and green water fluxes (evapotranspiration) ~~water~~
129 ~~fluxes, as well as and~~ the ecohydrological resilience to drought. ~~Here, ecohydrological resilience is defined here~~
130 as the ability of the soil–plant–water system to sustain–maintain key ecohydrological functions, including soil
131 moisture storage, transpiration, and groundwater recharge, key hydrological and ecological functions under
132 drought stress (Falkenmark & Rockström, 2006; Neill et al., 2021; Tetzlaff et al., 2024).

133
134 Sustainable land management also requires consideration of sensitivity to climate change, which is altering
135 hydroclimatic regimes by shifting precipitation patterns and increasing atmospheric moisture demand (Huntington,
136 2006; Trenberth, 2011). These changes can intensify drought frequency and duration, increase evaporative losses,
137 and reduce groundwater recharge and surface water availability, ~~thereby and thus~~ exacerbating water scarcity in
138 many regions (Ault, 2020; Yuan et al., 2023). Because land use practices—particularly forest management—are
139 expected to strongly influence water partitioning, it is important to assess their impacts under changing
140 hydroclimatic conditions in order to evaluate the ecohydrological resilience of soil–plant–water systems,
141 especially in drought-sensitive areas.

142 The understanding of how land use change affects runoff generation, soil moisture storage and evapotranspiration
143 dynamics has gradually developed through decades of research, including long-term paired experimental
144 watershed investigations of water yield (Bosch & Hewlett, 1982; Brown et al., 2005, 2013; Hibbert, 1967).
145 However, quantifying the impact of forest management on water partitioning remains challenging in most
146 situations (Guswa et al., 2020). This is due to the complex interplay of climate conditions, soil properties,
147 vegetation type, and topography, and the difficulty in distinguishing individual evapotranspiration (ET)
148 components (Kool et al., 2014; Smith et al., 2021; Zhang et al., 2001). These challenges are further compounded
149 by scarce long-term observational data for forest ecosystems, which are essential given their slow dynamics and
150 lengthy growth cycles (Tetzlaff et al., 2017).

151 In forest ecosystems, ET is particularly challenging to simulate due to complex interactions among canopy
152 structure, stomatal behavior, and root water uptake (Tague & Band, 2004). Many ecohydrological models include
153 some form of root water uptake parameterization (e.g., mHM, EcH2O-iso, RHESSys), in which canopy
154 transpiration is typically constrained by surface energy balance and stomatal conductance and subsequently

155 distributed among soil layers based on soil water availability and root distribution. While such models provide
156 detailed representations of land–atmosphere and soil–vegetation interactions, their application in forest
157 management studies is often constrained by high data requirements, computational demand, and parameter
158 uncertainty, particularly in data-scarce regions (Fatichi et al., 2012; Ricci et al., 2020; Tague & Band, 2004). In
159 this context, conceptual tracer-aided ecohydrological models can provide a complementary, process-based, and
160 practical framework for systematically exploring long-term forest management impacts on water partitioning and
161 ecohydrological resilience (Landgraf et al., 2023). By integrating climatic forcing, canopy structure (e.g., leaf area
162 index), soil moisture dynamics, and stable water isotopes, such approaches facilitate robust assessment of green-
163 and blue-water fluxes under contrasting forest management scenarios (Neill et al., 2021).

164 In this study, we apply the tracer-aided conceptual model EcoPlot-iso to assess how land use, specifically forest
165 management strategies, influences water partitioning and soil moisture storage in the drought-sensitive, lowland
166 Demnitzer Millcreek catchment, NE Germany. This lowland catchment is typical of large areas in central Europe
167 where freely draining, sandy soils combine with a relatively low precipitation, and high evaporative demand
168 amplify drought stress under climate change. To improve the quantification of transpiration, we introduce a novel
169 development in EcoPlot-iso by integrating a depth-dependent root water withdrawal function into the transpiration
170 equation. The model is dual-calibrated and validated using seven years of soil moisture data and three years of
171 soil water isotope data. A series of generic forest management scenarios — varying broad forest types (broadleaf,
172 coniferous, agroforestry), forest density, and rooting characteristics — are developed within a parsimonious,
173 tracer-aided forest management scenario framework, to explore their impacts on vertical water fluxes and
174 ecohydrological resilience.

175 This study aims to answer the following research questions:

- 176 ➤ How does vegetation cover influence water use and partitioning under varying wetness conditions
177 in a drought-sensitive, lowland catchment?
- 178 ➤ What are the implications of alternative generic forest management scenarios for water availability
179 and overall ecohydrological resilience?
- 180 ➤ How can ~~we optimize the~~ land management strategies ~~be optimized to reduce to mitigate~~ drought
181 impacts on soil water availability and groundwater recharge and enhance ecohydrological resilience
182 under in the face of climate change?
- 183 ➤

184 **2 Study area**

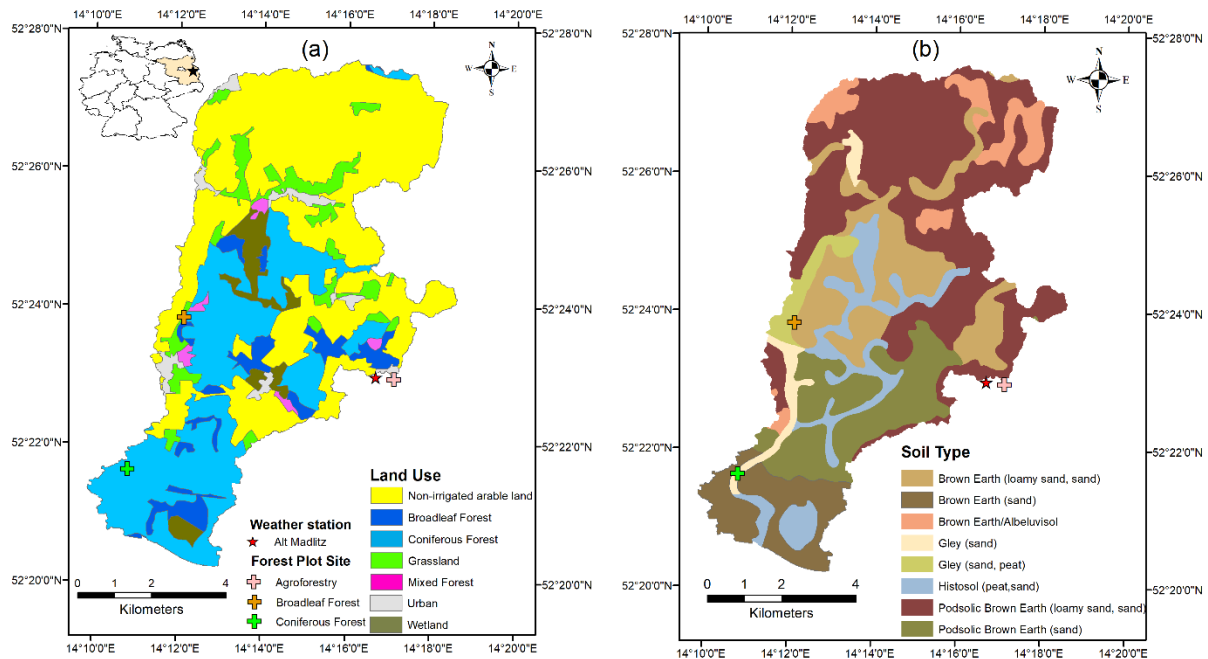
185 **2.1 Demnitzer Millcreek catchment (DMC)**

186 The Demnitzer Millcreek catchment (DMC) is a 66 km² lowland basin (30–90 m elevation) in the State of
187 Brandenburg, Germany, approximately 55 km east of Berlin (52°23' N, 14°15' E) (Fig. 1). Located in the Northern
188 European Plain, it is part of a drought-sensitive region that provides many essential ecosystem services, including
189 agriculture, timber production, and water supply.

190 The DMC landscape is dominated by non-irrigated farmland, mostly arable crops and some grazing on more
191 water-retentive ~~soils~~-brown earth and gley soils respectively which cover 60% of the catchment (Fig. 1a and b).
192 Forests cover 36% of the catchment on more freely draining sandy soils, and include coniferous, broadleaf, and
193 mixed stands. Small urban settlements (2%) are scattered throughout the catchment, with wetlands on peat soils
194 primarily found along streams in the central part of the catchment. The climate is temperate with warm summers,
195 with a mean annual temperature of 9.6°C and average precipitation of approximately 558 mm, based on weather
196 station data from 2000 to 2024. Potential evapotranspiration (PET) ranges from 584 to 789 mm per year from
197 2000 to 2024, based on calculations from this study (see Section 3.3). Interannual variability in precipitation,
198 including the identification of dry and wet years, is shown in Fig. S1, which highlights deviations from the long-
199 term mean and helps contextualize recent drought impacts. Rainfall peaks in summer, accompanied by intense
200 convective storms; however, surface runoff is rare, as the soils are highly permeable and dry in the growing season.
201 Consequently, the catchment is primarily groundwater-dominated with winter high flows and often dries in the
202 summer (Smith et al., 2021). The geology consists mainly of glacial and fluvial deposits and base moraines, while
203 the dominant soil types include poorly drained silty gley brown earth and well-drained podzolic brown earth soils
204 (Fig. 1b).

205 The DMC has a long history of human influence, with significant land use changes affecting its hydrology. In the
206 18th Century, artificial drainage channels were constructed to convert wetlands into agricultural land. Since the
207 1990s, efforts in wetland restoration and wildlife recolonization (e.g., beaver recovery) have aimed to enhance
208 water retention in the landscape. Long-term hydrological and isotopic monitoring (Gelbrecht et al., 1996, 2005;
209 Smith et al., 2020; Wu et al., 2021) has provided valuable insights into the impacts of agriculture and land use
210 management on water quality, ecohydrological partitioning and soil water storage. The 2018 European drought
211 and subsequent prolonged dry periods have exacerbated water scarcity and ecosystem vulnerability (Kleine et al.,
212 2021). In response, some land owners have explored agroforestry and other adaptive forest and tree management
213 strategies to improve water retention and reduce drought vulnerability~~landscape resilience~~ (Luo et al., 2024).
214 Agroforestry represents a transitional system blending low density tree cultivation ~~and~~ with agriculture; either in
215 terms of grazing the understory vegetation or crops (Landgraf et al., 2022; Quandt et al., 2023). Given the long-
216 term monitoring record and ongoing land use change, DMC serves as a useful site for assessing the impacts of
217 changing forest management on water partitioning, soil moisture and ecohydrological resilience under different
218 wetness conditions.

219



220
 221 **Figure 1.** Location, land use (a) and soil type (b) map of the Demnitzer Millcreek catchment, showing the current
 222 distribution of broadleaf forests, conifer forests, agroforestry, cropland, and grassland.

223 2.2 Forest Plot Sites

224 To investigate the effects of forest management scenarios on water partitioning and ecohydrological resilience,
 225 three predominantly forest plot sites — broadleaf forest, conifer forest and agroforestry — were selected within
 226 the drought-sensitive DMC. These plots represent contrasting forest types central to the modelling experiments.
 227 The plot locations are shown in Fig. 1, and key site characteristics are summarized below, with further details
 228 available in Kleine et al. (2021) and Landgraf et al. (2023). A summary of observed soil types and soil moisture
 229 monitoring characteristics for these three forest sites is provided in Table 1, which also highlights pronounced
 230 differences in long-term mean volumetric soil moisture averaged over the 0–1 m soil profile, with values highest
 231 in agroforestry (~21%), intermediate in broadleaf (~11%), and lowest in conifer forest (~5.5%).

232 The broadleaf forest site represents a relatively mature forest system (~60 years old) and is dominated by mature
 233 European oak (*Quercus robur*) with a few Scots pine (*Pinus sylvestris*) present within the plot. Additional species
 234 including Norway maple (*Acer platanoides*), elm (*Ulmus* spp.), and hazel (*Corylus avellana*) are found within
 235 10 m of the plot boundary. The soil is classified as **B**rown **e**Earth, with a loamy sand to sand texture.

236 The conifer forest site is structurally simpler and more homogeneous, and is dominated by mature Scots pine
 237 (*Pinus sylvestris*) plantation. A limited number of broadleaf species, such as European oak and Norway maple,
 238 are also present within the plot, reflecting a conifer-dominated canopy. The soil is a weakly developed brown
 239 earth, characterized by coarse sandy texture and overlying gravels.

240 The agroforestry site represents a transitional system between forest and agriculture and is characterized by
 241 minimal canopy cover and no irrigation. It consists of rows of small deciduous trees or shrubs (≤ 2 m in height),

242 spaced approximately 2–3 m apart, interplanted with rainfed legumes (Landgraf et al., 2023). The soil is classified
 243 as podsolc brown earth, with a loamy sand to sand texture.

244 Together, these three sites represent a realistic gradient of forest land use intensity and provide a basis for
 245 exploring how forest type, forest density, and rooting depth affect ecohydrological responses under varying
 246 climatic conditions.

247 **Table 1.** Summary of observed soil types and soil moisture data at the three forest sites.

Site	Soil Type	Texture	Layer	Soil Moisture (mm)				Period
				Max	Min	Mean	SD	
Broadleaf forest	Brown earth	Loamy sand/sand	0 to 10 cm	26.3	3.5	13.7	6.3	2018.6-2024.12
			10 to 30 cm	56.2	6.9	24.7	11.7	
			30 to 100 cm	147.5	25.8	71.7	33.5	
Conifer forest	Sandy brown earth	Coarse sand	0 to 10 cm	28.7	8.6	17.3	7.1	2019.3-2024.12
			10 to 30 cm	53.8	2.6	21.8	12.3	
			30 to 100 cm	34.7	2.7	15.9	8.0	
Agroforestry	Podsolc brown earth	Loamy sand/sand	0 to 10 cm	32.1	10.4	21.3	7.8	2019.3-2024.12
			10 to 30 cm	53.4	7.2	29.8	13.5	
			30 to 100 cm	223.6	86.8	163.4	42.0	

248 3 Method and Data

249 3.1 Model Framework and Structure

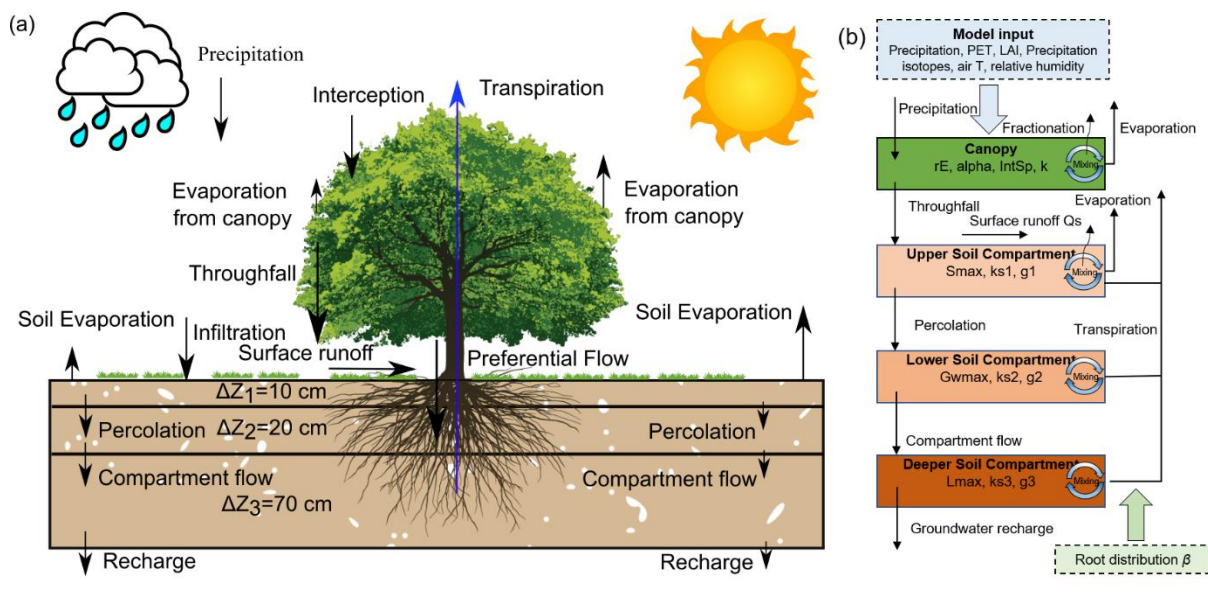
250 This study employs the EcoPlot-iso model, a tracer-aided ecohydrological modelling framework designed to
 251 simulate key ecohydrological and isotopic processes that characterise water partitioning at the plot scale (Birkel
 252 et al., 2024; Landgraf et al., 2023; Stevenson et al., 2023). EcoPlot-iso is a process-based conceptual model that
 253 simulates key ecohydrological fluxes, including interception, throughfall, infiltration, preferential flow, surface
 254 runoff, percolation, and groundwater recharge, as well as evapotranspiration components such as canopy
 255 evaporation, soil evaporation, and transpiration (Fig. 2a). These processes are represented within a vertical
 256 structure comprising a single canopy layer and three soil layers (0–10 cm, 10–30 cm, and 30–100 cm) (Fig. 2b).
 257 The vertical discretization follows the established EcoPlot-iso configuration and effectively represents vertical
 258 gradients in soil moisture and isotopic composition, broadly consistent with soil moisture and isotope
 259 measurements within each layer. Recently, the isotope tracking module was further developed to include
 260 fractionation and mixing processes, allowing EcoPlot-iso to better constrain the partitioning between evaporation
 261 and transpiration and improve water flux estimates. The required input variables (Table 2) include meteorological
 262 data such as precipitation, potential evapotranspiration (PET), air temperature, and relative humidity, along with
 263 stable water isotopic data (precipitation isotope) and vegetation-related parameters (leaf area index, LAI).

264 In EcoPlot-iso, canopy surface cover fraction (SCF) is derived from LAI using Beer’s law with an extinction
 265 coefficient rE (Eq. S1). Maximum canopy storage is determined by the SCF and an interception threshold
 266 parameter α . Interception is represented by a nonlinear saturation-type function (Eq. S2), whereby precipitation is
 267 first stored in the canopy until maximum canopy storage is reached, and any excess is routed as throughfall.
 268 Potential evapotranspiration PET is partitioned into canopy and soil fractions according to SCF (Eqs. S3 and S4).
 269 The canopy fraction drives evaporation from the interception store and transpiration from the soil layers, while
 270 the soil fraction drives evaporation from the upper soil layer (Eqs. S5–S6). Actual fluxes are constrained by water

289 availability: interception evaporation depends on canopy storage, transpiration is sequentially satisfied from the
 290 upper to deeper soil layers according to the relative soil-moisture availability (STO/S_{max}) of each layer (Eqs. S7–
 291 S9), and soil evaporation is limited by moisture availability in the upper soil. Surface runoff is represented using
 292 a Hortonian threshold approach, where precipitation in excess of infiltration capacity is routed as runoff (Eq. S10).
 293 Preferential flow is triggered when throughfall exceeds a threshold, with a calibrated parameter controlling the
 294 bypass proportion (Eq. S11). Percolation, compartment flow and groundwater recharge are represented as storage–
 295 discharge relationships, where outflows are parameterised as power functions of soil or groundwater storage (Eqs.
 296 S12-S14). Groundwater recharge is defined as the downward percolation flux at the lower boundary of the soil
 297 domain (30–100 cm layer), corresponding to a total soil depth of 1 m. Full variable definitions and governing
 298 equations are provided in Table S1 of the Supplementary Material (Eqs. S1–S14).

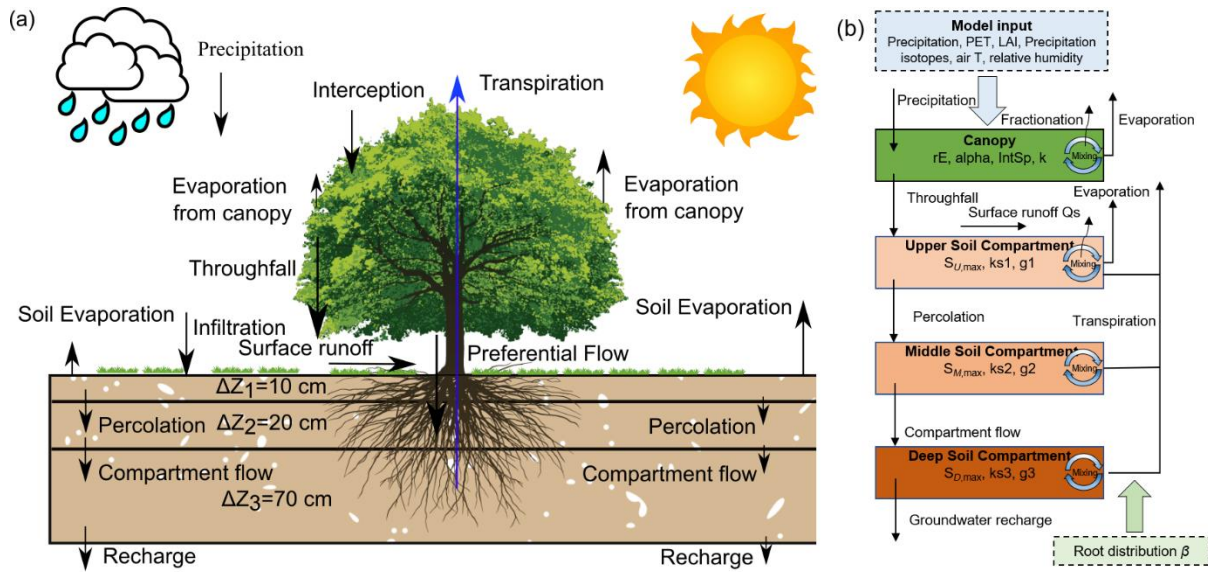
299 EcoPlot-iso has been applied in diverse climatic and hydrological settings, including a one-year simulation in
 300 Scotland (Stevenson et al., 2023), a one-year simulation at the Demnitzer Millcreek (DMC) site in the Northern
 301 European Plain (Landgraf et al., 2023), and a four-year simulation in the humid tropics of Costa Rica (Birkel et
 302 al., 2024). Building on these applications, this study employs EcoPlot-iso for a long-term tracer-aided
 303 ecohydrological simulation to assess the effects of different forest management scenarios on water partitioning
 304 and ecohydrological resilience.

305



306

Formatte



329

330 **Figure 2.** (a) Schematic representation of the ecohydrological fluxes and water partitioning in the EcoPlot-iso
 331 model illustrating major water fluxes and storage components; (b) Conceptual framework and key parameters of
 332 the EcoPlot-iso model (Landgraf et al., 2023; Stevenson et al., 2023), highlighting the key ecohydrological
 333 processes simulated in this study.

334 3.2 Model Adaptations: Integrating Root Distribution into the Transpiration Equation

335 Although root water uptake plays a critical role in soil–plant–atmosphere interactions, the vertical rooting
 336 distribution and the associated depth-dependent uptake efficiency was/were not explicitly represented in EcoPlot-
 337 iso (Stevenson et al., 2023). The current study introduces a novel depth-dependent root uptake function to improve
 338 the model’s simulation of transpiration and water partitioning across different root distributions. This adaptation
 339 enables the model to account for variations in rooting depth and water uptake efficiency across land use types—
 340 such as young and mature forests or contrasting vegetation covers—that affect soil water extraction. Specifically,
 341 a new transpiration equation was implemented to calculate root water uptake across three soil compartments—
 342 shallowupper, middle, and deep—by incorporating depth-specific uptake efficiency:

$$343 \quad T_{p1} = r_{L1} * (T_P - E_i) * \left(\frac{S_U}{S_{U,max}} \right) \quad (1)$$

$$344 \quad T_{p2} = r_{L2} * (T_P - E_i - T_{p1}) * \left(\frac{S_M}{S_{M,max}} \right) \quad (2)$$

$$345 \quad T_{p3} = r_{L3} * (T_P - E_i - T_{p1} - T_{p2}) * \left(\frac{S_D}{S_{D,max}} \right) \quad (3)$$

346 where T_{p1} , T_{p2} , T_{p3} represent the transpiration from the upper, middlelower, and deeper soil compartments,
 347 respectively. T_e denotes the canopy fraction of potential evapotranspiration. E_i denotes the canopy evaporation.
 348 S_U^{FO} , S_M^{GW} , S_D^{deep} represent the water storage in the upper, middlelower, and deeper soil compartments. $S_{U,max}$,
 349 $S_{M^{GW},max}$, $S_{D^{deep},max}$ are the maximum water storage capacities of these compartments. r_{L1} , r_{L2} and r_{L3} represent
 350 the root water withdrawal efficiency in the upper, middlelower, and deeper soil compartments, respectively.

389 To explicitly link root water uptake to soil moisture availability and transpiration demand, an efficiency factor $r(z)$
390 was introduced. The exponential root water withdrawal efficiency function is defined as:

391
$$r(z) = e^{-\beta z} \tag{4}$$

392 where $r(z)$ represents the capacity of roots to extract water at depth z , and β is the decay rate (m^{-1}), which
393 determines how quickly root activity decreases with increasing depth. A higher β value concentrates root activity
394 near the surface, while lower β values allow for deeper water uptake (see Fig. S2 in Supplement). This formulation
395 builds on the common assumption that potential root water uptake decreases exponentially with depth (Li et al.,
396 1999; Wu et al., 1999) and is intentionally simplified for a plot-scale, data-constrained model setup. The soil
397 profile is discretized into three layers (0–10 cm, 10–30 cm, and 30–100 cm; Fig. 2a), and $rL1$, $rL2$, and $rL3$ are
398 calculated by evaluating $r(z)$ at the midpoint depth of each layer ($z = 5, 20, \text{ and } 65$ cm, respectively). These layer-
399 specific efficiency values are then used as weighting coefficients in Eqs. (1)–(3) to calculate transpiration from
400 each of the three soil compartments.

401 3.3 Model Setup, ~~and~~ Input and Observation Data

402 The EcoPlot-iso model was applied to DMC across five sites with different dominant land use: broadleaf forest,
403 conifer forest, agroforestry, cropland and grassland over a 25-year period (2000–2024) at daily timesteps. Soil
404 moisture initialization was based on observed data, and a one-year spin-up period was included before each
405 simulation to stabilize initial conditions. The input datasets required for the model—climate, vegetation, soil
406 moisture, and stable water isotope data—are summarized in Table 2. Climate variables, including precipitation,
407 temperature, wind speed, and relative humidity, were primarily obtained from the Müncheberg weather station
408 (DWD, German Weather Service, ~20 km from DMC). Potential Evapotranspiration (PET) was calculated using
409 the FAO Penman-Monteith equation, while net radiation was derived from ERA5 reanalysis data (Hersbach et al.,
410 2020). The Leaf Area Index (LAI) time series was extracted from the MODIS 8-day LAI product at the location
411 of each study site and linearly interpolated to daily timesteps. To improve accuracy and reduce data noise, the
412 MODIS LAI was further bias-corrected against in-situ LAI measurements (maximum and minimum values),
413 following Smith et al. (2021) and Wu et al. (2023). Given the plot-scale setup of EcoPlot-iso, agroforestry systems,
414 characterized by mixed crop–tree vegetation, are represented implicitly using MODIS-derived LAI and calibration
415 against plot-scale soil moisture and isotope observations, rather than explicitly resolving multiple vegetation types.
416 In addition, the complete set of time series input data used to drive the EcoPlot-iso simulations in the Demnitzer
417 MillCreek Catchment for 2000-2024—including daily precipitation, precipitation isotopes ($\delta^2\text{H}$), air temperature,
418 relative humidity, Leaf Area Index (LAI), and potential evapotranspiration (PET)—is presented in Figure S3 of
419 the Supplementary Material.

420 Surface soil moisture (0–10 cm) was measured using a handheld soil moisture device (Theta handheld probe ML3
421 Sensor) on a monthly basis during two field observation periods (2018–2019 and 2021). For subsurface soil
422 moisture, permanently installed ~~soil moisture~~ probes were used: SMT-100 at forest and grassland sites, and CS650
423 at agroforestry and cropland sites. Measurements were recorded at 15-minute intervals with two replicates per
424 depth. To facilitate data processing and consistency, all soil moisture datasets were aggregated into daily mean
425 values, resulting in one volumetric water content value per site and soil depth. Details of the measurement devices,
426 depth intervals, and aggregation methods ~~is-are~~ summarized in Table S2. Daily precipitation samples for stable

427 water isotope analysis from June 2018 onward were collected at the Hasenfelde AWS, and earlier data were
 428 obtained from the Berlin weather station. Soil water isotopes were sampled from bulk soil at the four plot sites at
 429 five depths (0–5, 5–10, 10–20, 20–30, and 30–50 cm) every 3–4 weeks during the growing season. The isotope
 430 data were aggregated according to the thickness of the corresponding model soil compartments. All isotope values
 431 are reported relative to Vienna Standard Mean Ocean Water (VSMOW). Further details on site instrumentation
 432 and data collection are described in Landgraf et al. (2022).

433 **Table 2.** Summary of the used climate, vegetation, soil moisture, and isotope data.

Data	Unit	Period	Timestep	Acquisition
<i>Climate data</i>				
Precipitation	mm/d	2000-2024	Daily	Muencheberg weather station (52.52°, 14.12 °)
Temperature	°C			
Windspeed	m/s			
Relative humidity	%		Hourly	ERA5
Net shortwave radiation	W/m ²			
Net longwave radiation				Daily
Potential evapotranspiration	mm/d			
<i>Vegetation data</i>				
Leaf area index	-	2000-2024	8-days	MODIS at broadleaf forest, coniferous, and agroforestry sites
<i>Soil data</i>				
Soil moisture	%	2018-2024	Daily	broadleaf forest, cropland, agroforestry, and grassland sites
<i>Isotope data</i>				
Precipitation isotope $\delta^2\text{H}$	‰	2000-2024	Daily	Hasenfelde (52.41°N, 14.19°E), weather station in Berlin
Soil water isotope		2018-2019, 2021	Daily	Manually at broadleaf forest, cropland, agroforestry, and grassland sites

434

435 3.4 Model Calibration and Validation

436 The EcoPlot-iso model was calibrated using the Monte Carlo approach combined with a multi-criteria evaluation
 437 based on soil moisture and soil water isotope observations at each land use site. For each calibration, 100,000
 438 parameter sets were generated using the Latin Hypercube Sampling (LHS) within a Monte Carlo framework
 439 (McKay et al., 1979) to broadly sample the parameter space and capture a wide range of plausible model behaviors.

440 The initial parameter ranges were defined based on a literature values and site-specific knowledge. Specifically,
 441 initial ranges for the radiation extinction factor (rE) were guided by vegetation-specific light attenuation
 442 coefficients from canopy gap-fraction theory (Larcher, 1975; Gigante et al., 2009), using typical reference values
 443 of 0.35 for grasslands, 0.45 for croplands, and 0.65 for forests. Initial ranges for the interception storage capacity
 444 parameter (α) were guided by scaling values reported in global syntheses of canopy interception storage (Zhong
 445 et al., 2022) and interception sensitivity studies (Barnard et al., 2014), accounting for differences in model time
 446 step and formulation. The resulting interception evaporation is consistent with observational studies indicating
 447 that canopy interception losses typically represent approximately 10–30% of annual precipitation in forested
 448 systems (Staelens et al., 2008; Llorens & Domingo, 2007).

485 Model performance was evaluated using the modified Kling-Gupta Efficiency (*mKGE*) (Kling et al., 2012),
486 calculated separately for soil moisture (*mKGE_{sm}*) and soil water isotopes (*mKGE_{iso}*) at each of the three soil depth
487 layers. Calibration followed a two-step refinement process. In the first step, based on the initial parameter ranges,
488 parameter sets were retained only if they fell within the intersection of the top 60th percentile of all six individual
489 *mKGE* metrics (i.e. soil moisture and soil water isotopes at each of the three soil depths). This step substantially
490 reduced the number of parameter sets from the initial 100,000 samples. This intersection-based filtering ensured
491 that retained simulations performed consistently well across all evaluated variables and depths. By retaining only
492 the performance metrics and corresponding parameter sets, this step efficiently screened the parameter ~~sets space~~
493 while substantially reducing data storage requirements during the initial exploration.

494 In the second step, the model was re-run using the retained parameter ~~sets space~~—obtained from Step 1. For these
495 re-run simulations, an average *mKGE* value across depths and variables was then used as the objective
496 performance metric (Eq. 5), and the 100 best-performing simulations were selected for final analysis. The model
497 parameters, their initial ranges, and the refined ranges for each of land use are summarized in Table S3 in the
498 Supplement. To assess parameter constraints and equifinality, the probability density distributions and median
499 values of the calibrated parameters were derived from the 100 best-performing simulations for each site (see Fig.
500 S4). These were then used to evaluate the convergence of the parameters relative to their initial ranges.

$$501 \quad mKGE = \frac{\sum_i^3 mKGE_{sm} + \sum_i^3 mKGE_{iso}}{6} \quad (5)$$

502 Model parameters were calibrated using the full available observation, comprising seven years of soil moisture
503 data and three years of soil water isotope data, in order to maximise information content under limited isotope
504 availability (Shen et al., 2022). To additionally assess model robustness beyond a shorter calibration window, a
505 split-sample calibration–validation experiment was conducted consistently across all land-use types. In this
506 experiment, the model was calibrated using an earlier subset of the soil moisture and isotope observations,
507 followed by validation against an independent soil moisture period, as isotope observations were not available for
508 validation. Results from this split-sample evaluation, which showed good parameter transferability across most
509 sites, are reported in Table S4 and Figures S5–S7 of the Supplement. Given this transferability, the full-period
510 calibration was retained for the main scenario simulations, as it provides more stable parameter estimates under
511 data limitations, while the split-sample results are presented for transparency and robustness assessment.

512 **3.5 Development and Application of a Generic Forest Management Scenario Framework**

513 The primary goal of this study was to develop a new, parsimonious and generic forest management scenario
514 framework to evaluate how forest type, forest density, and root distribution —associated with forest age—
515 influence long-term water partitioning and ecohydrological resilience under comparable environmental conditions.
516 This framework was designed to capture the dominant effects of vegetation structure—such as interception and
517 transpiration through canopy and root networks—on water partitioning, rather than to reproduce detailed species-
518 specific physiology.

519 Based on this conceptual framework, baseline simulations covering the period 2000-2024 were established using
520 EcoPlot-iso model at three forest sites within the DMC (broadleaf forest, conifer forest, and agroforestry). These

560 baseline simulations provide forest-type-specific reference conditions against which alternative management
561 scenarios were evaluated.

562 To isolate the effects of forest management from site-specific soil properties and boundary conditions, we
563 extended the observed forest-site configurations by systematically combining ~~each~~ forest-type-specific vegetation
564 parameter sets with ~~each~~ site-specific soil parameter sets, derived from the corresponding baseline calibrations,
565 resulting in a 3×3 scenario matrix (Fig. 3). The diagonal entries represent the observed site-based reference
566 configurations—namely, Broadleaf forest site, Conifer forest site, and Agroforestry site—and are therefore
567 treated as baseline scenarios. The remaining cross-combinations represent hypothetical but plausible forest-site
568 (soil) configurations, in which vegetation characteristics are applied to alternative site-specific soil hydraulic
569 properties and boundary conditions (e.g., soil texture and compaction). This design enables vegetation effects to
570 be assessed independently of site-specific controls for scenario analysis, while ~~explicitly~~ acknowledging that
571 vegetation and soil controls may not be fully independent and that soil hydraulic properties and boundary
572 conditions remain inherently site-dependent. Ensemble-based comparisons across site configurations for each
573 forest type therefore support a more robust and generic interpretation of ecohydrological behaviour.

574 Specifically, for each of forest-site baseline scenario calibration, we retained the top 100 best-performing
575 simulations—ranked by average mKGE—and their corresponding parameter sets (as described in Section 3.4).
576 Forest-type-specific vegetation parameters (e.g., rE , α) were derived from site-specific calibrations for broadleaf,
577 conifer, and agroforestry systems, and their median values from the 100 best-performing simulations at each site
578 were used to represent characteristic vegetation conditions. The root distribution parameter (β) was not treated as
579 strictly vegetation-specific, but as jointly influenced by vegetation type, soil properties, and soil water availability
580 (Fig. S4). This ensemble-based selection was used to reduce parameter uncertainty and equifinality effects. These
581 calibrated parameter sets were then used for subsequent scenario simulations to ensure physically consistent
582 parameter configurations across all forest types. In contrast, soil-related parameters (e.g., $ks1$, $ks2$, $ks3$, $S_{U,max}$,
583 $S_{M,max}$, $S_{D,max}$, I_c , $g1$, $g2$, $g3$, $PFscaleS_{max}$, GW_{max} , L_{max}) were retained from the corresponding forest sites to
584 preserve site-specific hydraulic properties and boundary conditions.

585 For vegetation forcing, we used forest-type-specific observed LAI time series (broadleaf, coniferous, and
586 agroforestry), derived from the MODIS LAI products, described in Section 3.3 (Table 2; Fig. S3d). Forest-type-
587 specific initial soil moisture conditions for the three soil layers were kept consistent with the corresponding
588 baseline simulations. All scenario simulations were driven using identical climate input data, precipitation isotope
589 time series, and potential evapotranspiration forcing as the baseline simulations to isolate the effects of forest
590 characteristics and management.

591 The scenario framework varied three key dimensions of forest management:

- 592 a) Forest type was varied by implementing three canopy types—broadleaf, conifer, and agroforestry—each
593 assigned type-specific vegetation parameters and LAI time series to reflect differences in canopy
594 structure.
- 595 b) Forest density was varied by multiplying the reference LAI by a scaling factor ranging from 0.2 to 1.8.
596 Higher forest density was represented by scaling factors >1.0 , indicating denser canopy cover, while
597 lower forest density corresponded to factors <1.0 , reflecting more open canopy conditions. The applied
598 LAI scaling range (0.2–1.8) follows previous tracer-aided modelling approaches (Neill et al., 2021) and

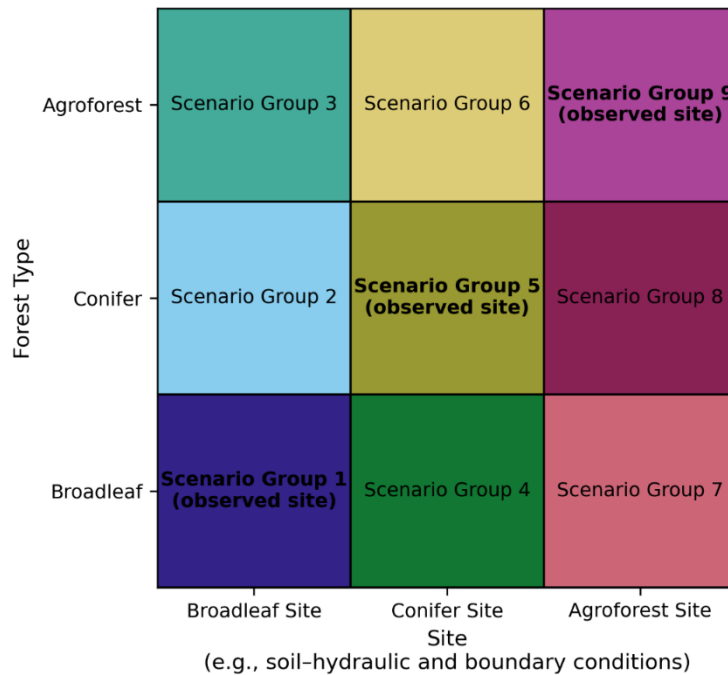
599 spans realistic management-induced variability in canopy density, while remaining consistent with
600 reported LAI values for mature European forests (Leuschner et al., 2006).

601 c) Root water uptake efficiency was varied by scaling the site-calibrated β parameter to represent
602 contrasting vertical root distributions associated with forest developmental stage. Three rooting scenarios
603 were considered: $0.5 \times \beta$, $1.0 \times \beta$, and $2.0 \times \beta$, where β is the calibrated value for each forest site. Lower
604 scaled values ($0.5 \times \beta$) represent more developed forests with deeper, less surface-weighted rooting
605 systems, while higher scaled values ($2.0 \times \beta$) represent younger or less-developed forests with shallower,
606 more surface-weighted rooting distributions (see Fig. S1). The $1.0 \times \beta$ scenario corresponds to the
607 observed rooting distribution at each forest site.

608 Within this framework, LAI and rooting distribution were treated as independent scenario dimensions. LAI scaling
609 represented management-induced changes in canopy density, whereas rooting distribution scenarios reflected
610 contrasts in belowground water uptake. Their combined effects on water fluxes were evaluated without assuming
611 a fixed linkage between canopy structure and rooting depth. This separation acknowledges that canopy density
612 can change rapidly through management (e.g., thinning or harvesting), while rooting characteristics typically
613 reflect longer-term stand development, thereby allowing realistic representation of above- and belowground
614 controls on water partitioning.

615 Although EcoPlot-iso was originally developed for plot-scale applications, it is applied here to represent
616 ecohydrological fluxes in a range of well-characterized sites within the DMC region. The model employs a one-
617 dimensional approach that does not explicitly account for lateral fluxes; however, this simplification is intentional.
618 It enables clearer interpretation of process-level dynamics under contrasting vegetation and climate conditions,
619 making it suitable for general scenario analysis. This assumption is especially justified in the DMC catchment,
620 which is characterized by flat, lowland topography and is predominantly governed by vertical hydrological fluxes
621 (Kleine et al., 2021; Smith et al., 2020).

622 The framework is not intended to reproduce exact spatial patterns or detailed species-specific physiology, but
623 rather to capture the dominant effects of vegetation structure on vertical water fluxes and soil moisture dynamics.
624 By focusing on variations in forest type, forest density, and root distribution associated with forest age and
625 management, the framework enables a generalized assessment of long-term water partitioning and
626 ecohydrological resilience under comparable environmental conditions. As such, it provides a practical and
627 transferable tool for evaluating forest management impacts on water availability and ecohydrological resilience
628 in drought-sensitive lowland catchments.



629

630 **Figure 3.** Matrix of nine Scenario Groups formed by combining three site-specific configurations (Broadleaf Site,
 631 Conifer Site, and Agroforest Site) with three forest types (Broadleaf, Conifer, and Agroforest). Each colored block
 632 represents a Scenario Group consisting of multiple sub-scenarios (e.g., varying forest densities and root water
 633 uptake distributions). Diagonal entries (Scenario Groups 1, 5, and 9), marked as “observed configuration”,
 634 correspond to forest–site combinations observed at the field sites, where vegetation type and site-specific soil–
 635 hydraulic and boundary conditions are consistent with real-world conditions.

636 **4 Results**

637 **4.1 Dynamics of Soil Moisture and Soil Water Isotopes at the Broadleaf Forest Site**

638 Figure 4 shows the 25-year baseline simulations of soil moisture and soil water isotopes dynamics at the broadleaf
 639 forest site at a daily time step as an example. In general, the model effectively captures the magnitude, variability,
 640 extremes, and timing of soil moisture dynamics. Surface soil moisture shows higher variability than deeper layers.
 641 Based on the modified Kling-Gupta Efficiency (mKGE), soil moisture simulations generally perform better in the
 642 deep layer than in the upper shallow- and middle lower-layers, though this may partly reflect the more limited
 643 variance in deeper soil moisture. In addition, the model slightly overestimates low soil moisture in the deeper
 644 layers during wet summers (e.g., 2023, 2024) and underestimates soil moisture during dry winters (e.g., 2021 and
 645 2022). Soil water isotope simulations also perform well, with higher mKGE values in the middle intermediate
 646 layer than in surface upper and deeper layers. The uncertainty range of soil water isotope simulations is narrower
 647 than that of soil moisture, indicating lower uncertainty in the isotope predictions.

648 Table 3 shows the modified Kling-Gupta Efficiency (mKGE) and Root Mean Square Error (RMSE) values for
 649 soil moisture and soil water isotopes across different land use plots. In all other cases the mKGEs for soil moisture
 650 are similar to the broadleaved plot, and soil water isotopes are reasonably reproduced, indicating the model’s
 651 robustness and transferability. These results provide strong support for the appropriateness of applying EcoPlot-
 652 iso to assess the impacts of alternative forest management scenarios in subsequent analyses. In addition, simulated
 653 evapotranspiration was independently evaluated against MODIS-derived ET for all land use types, with model

654 performance quantified using RMSE and mKGE metrics (Table S4). This independent evaluation provides further
 655 support for the model's ability to reproduce key water fluxes beyond the variables used for calibration.

656 **Table 3.** Model performance metrics for soil moisture and soil water isotopes ($\delta^2\text{H}$) at each land use site over the
 657 full evaluation period (2000–2024), evaluated using the modified Kling–Gupta Efficiency (mKGE) and the root
 658 mean square error (RMSE, mm for soil moisture and ‰ for $\delta^2\text{H}$). Metrics are computed by comparing observed
 659 and simulated time series at each soil depth.

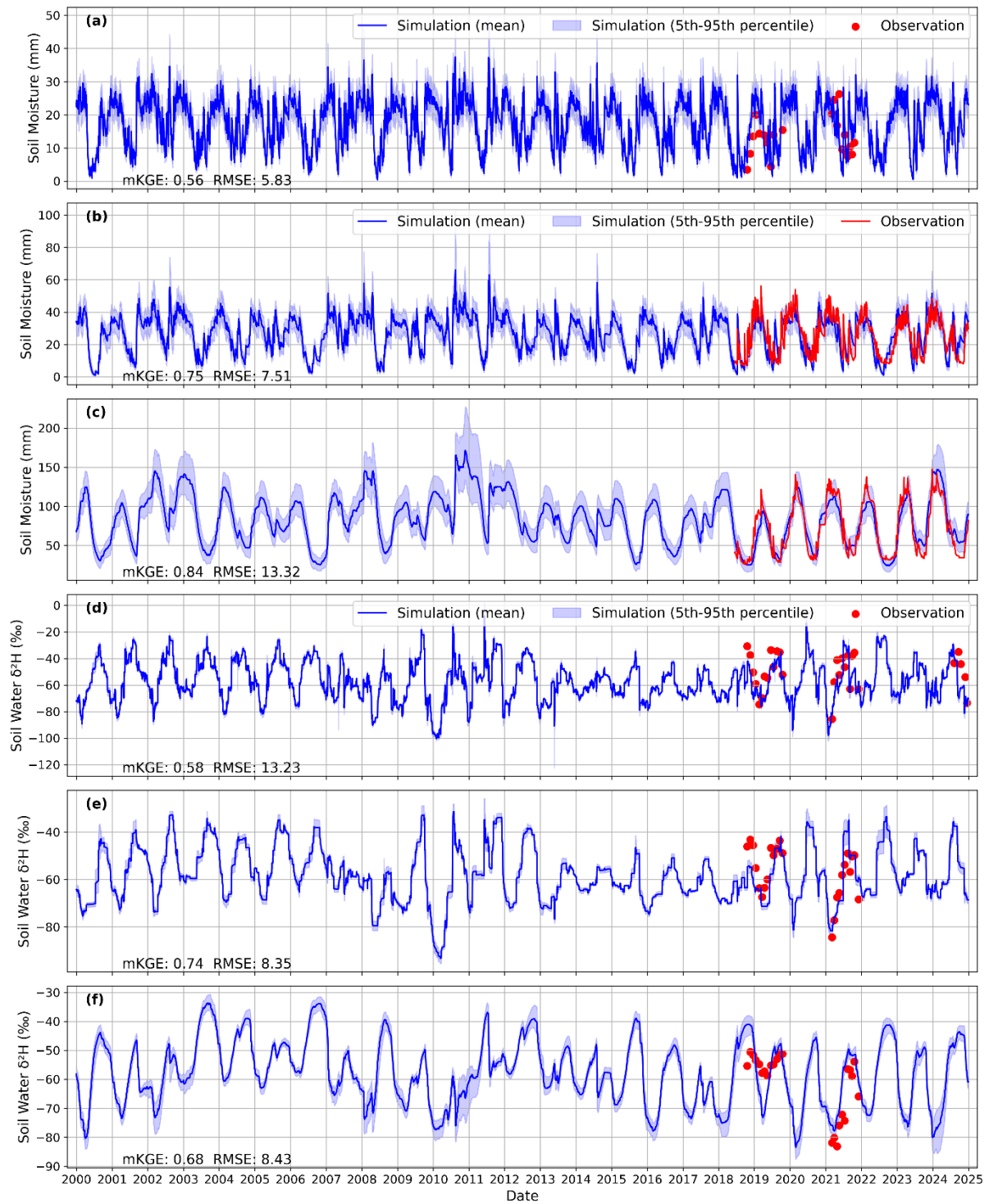
Sites	Soil moisture						Soil water isotope ($\delta^2\text{H}$)					
	Upper		<u>Middle</u>	<u>Lower</u>	Deep		Upper		<u>Middle</u>	<u>Lower</u>	Deep	
	<u>m</u> KGE	RMSE	<u>m</u> KGE	RMSE	<u>m</u> KGE	RMSE	<u>m</u> KGE	RMSE	<u>m</u> KGE	RMSE	<u>m</u> KGE	RMSE
Broadleaf Forest	0.56	5.83	0.75	7.51	0.84	13.32	0.58	13.23	0.74	8.35	0.68	8.43
Conifer forest	0.61	5.77	0.68	8.68	0.70	5.56	0.67	11.69	0.80	6.94	0.50	13.09
Agroforestry	0.72	5.22	0.79	6.63	0.77	23.43	0.82	8.09	0.85	10.45	0.79	8.98
Grassland	0.89	1.67	0.71	6.18	0.72	16.01	0.71	9.07	0.77	7.69	0.61	8.36
Cropland	0.53	5.84	0.62	8.88	0.71	22.36	0.83	8.36	0.85	9.19	0.36	13.71

660

661

662

663



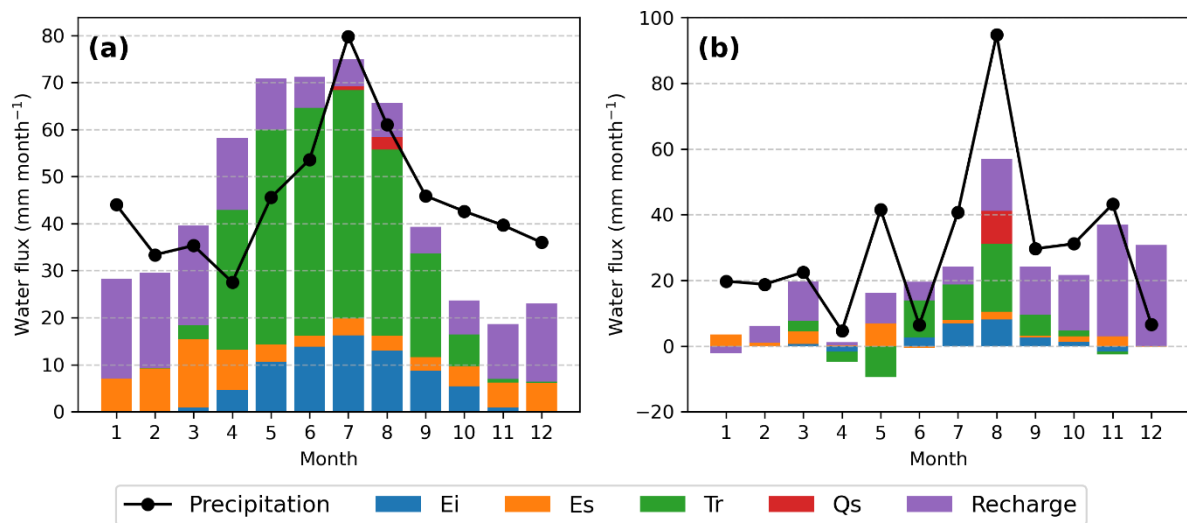
664
665
666
667
668
669
670
671
672

Figure 4. Long-term (2000–2024) simulations of soil moisture and soil water isotope ($\delta^2\text{H}$) at three different depths using EcoPlot-iso at a broadleaf forest site in the Demnitzer Millcreek catchment. (a–c) Simulated (mean \pm 5th–95th percentile) and observed soil moisture at surface (0–10 cm), lower (20–30 cm), and deeper (30–100 cm) layers. (d–f) Simulated (mean \pm 5th–95th percentile) and observed soil water isotopic composition ($\delta^2\text{H}$) at corresponding depths. The blue line represents the mean value of the 100 best simulations, while the shaded area indicates the range between the 5th and 95th percentiles of these simulations. The red points and red line represent observed values. Modified Kling-Gupta Efficiency (mKGE) values for each simulation are indicated in the respective panels.

673 **4.2 Water Balance Components Under Different Wetness Conditions at the Broadleaf Forest Site**

674 Figure 5 presents the mean monthly water balance components and their changes between dry and wet years for the
 675 the baseline simulation at the broadleaved forest site from 2000 to 2024. Groundwater recharge dominates blue
 676 water fluxes, while surface runoff is rare and occurs only during extreme summer rainfall events (Fig. 5a).
 677 Transpiration and canopy evaporation dominate in summer, while soil evaporation peaks in spring. Across dry
 678 and wet years, groundwater recharge shows the strongest sensitivity to interannual wetness, with reduced recharge
 679 during dry years and enhanced recharge during wet years following precipitation anomalies (Figs. 5b and S1). In
 680 contrast, transpiration remains relatively stable despite differences in annual wetness, indicating resilient
 681 vegetation function. This stability likely reflects the mature age of the forest (~60 years), although gradual changes
 682 in forest structure over the 20-year period may also play a role. Corresponding water balance results for the conifer
 683 forest and agroforestry sites are provided in the Supplementary Material (Fig. S9). Across the three forest types,
 684 the conifer forest exhibits the largest changes in groundwater recharge between dry and wet years, particularly in
 685 August, whereas agroforestry shows comparatively smaller changes than the broadleaf forest, indicating higher
 686 ecohydrological resilience. Overall, these seasonal patterns offer key insights into water partitioning under three
 687 forest baseline conditions and establish an important baseline for evaluating the impacts of alternative forest
 688 management scenarios.

689



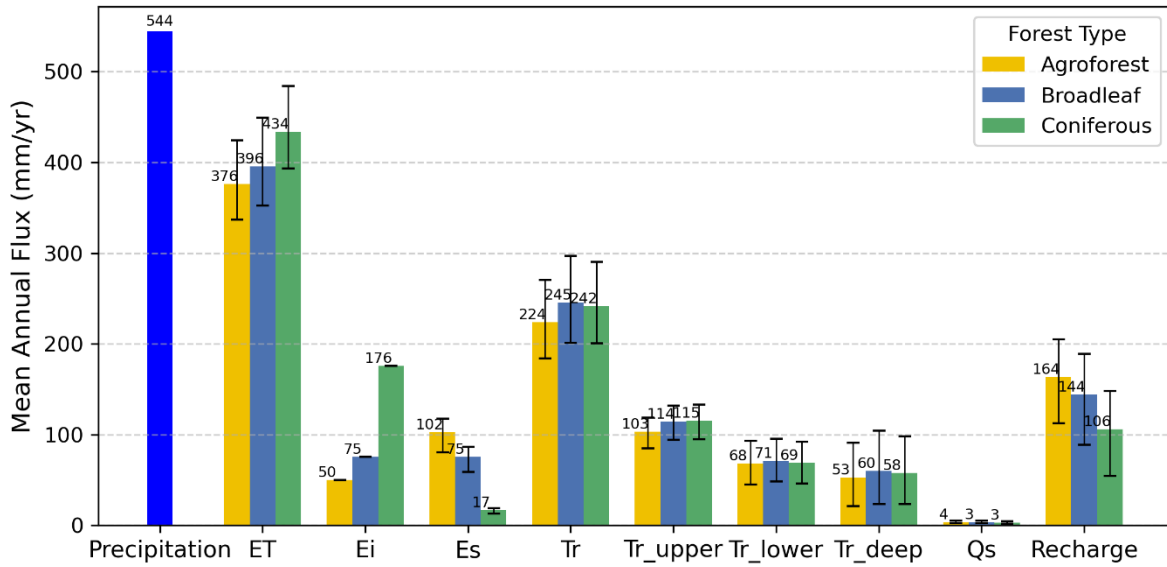
690 **Figure 5.** Mean monthly water balance components for the broadleaf forest site in the Demnitzer Millcreek
 691 catchment over 2000–2024, simulated with EcoPlot-iso using the mean of the best 100 parameter sets (see Section
 692 3.4 for details). Stacked bars show monthly totals of interception evaporation (Ei), soil evaporation (Es),
 693 transpiration (Tr), surface runoff (Qs), and groundwater recharge, while the black line indicates precipitation (P).
 694 (a) Long-term mean monthly water balance (mm month⁻¹). (b) Differences between wet years (2002, 2007, 2010,
 695 2023) and dry years (2006, 2018, 2022), expressed as wet minus dry (mm month⁻¹).
 696
 697

698 **4.3 Impacts of Forest Management on Water Partitioning and Soil Moisture**

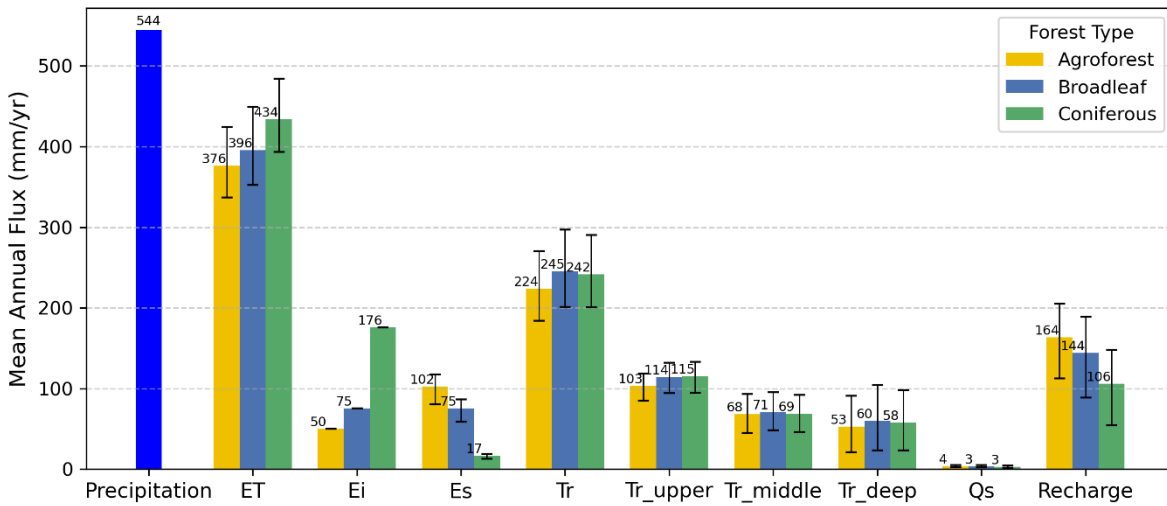
699 Results in this section are based on the full forest management scenario framework, including all nine forest–site
 700 Scenario Groups and their associated ensemble simulations (Fig. 3), rather than on the observed baseline
 701 configurations alone.

702 4.3.1 Water Balance and Partitioning Across Forest Types

703 Figure 6 compares the mean annual water balance components across broadleaf forest, coniferous forest, and
704 agroforestry types based on the ensemble mean of simulations derived from the paired vegetation–site soil
705 parameter configurations (Fig. 3), under reference canopy and rooting conditions (LAI scaling = 1; $\beta = 1 \times \beta$).
706 Results showed that evapotranspiration under coniferous forests accounted for 7% more of annual precipitation
707 than broadleaf forest, and 11% more than in agroforestry systems. This was primarily due to higher transpiration
708 (Tr) and canopy interception evaporation (Ei). ~~In-Accordingly, contrast,~~ soil evaporation (Es) and groundwater
709 recharge (Recharge) were lowest in conifers and highest in agroforestry. Agroforestry had 11% more groundwater
710 recharge relative to annual precipitation than conifers, and 4% more than broadleaf forests. Across forest types,
711 the largest fraction of transpiration originated from the upper soil layer (Tr_uUpper), reflecting its closer coupling
712 to precipitation inputs and higher soil moisture availability, while surface runoff (Qs) remained minimal and
713 nearly identical. These results reflect the influence of forest structure and canopy cover on ecohydrological
714 partitioning, with coniferous systems favoring atmospheric losses and agroforestry promoting soil evaporation
715 and subsurface recharge. They underscore the trade-offs between evapotranspiration and groundwater recharge
716 across different forest types.



717



718

719 **Figure 6.** Comparison of mean annual water balance components across different forest types: broadleaf (blue),
 720 coniferous (green), and agroforestry (yellow). Bars represent the mean annual flux based on 25-year totals, with
 721 error bars indicating the 5th and 95th percentile ranges of the 100 best simulations. All simulations were conducted
 722 under baseline conditions with a fixed forest root parameter β of 0 and LAI scaling factor of 1.0.

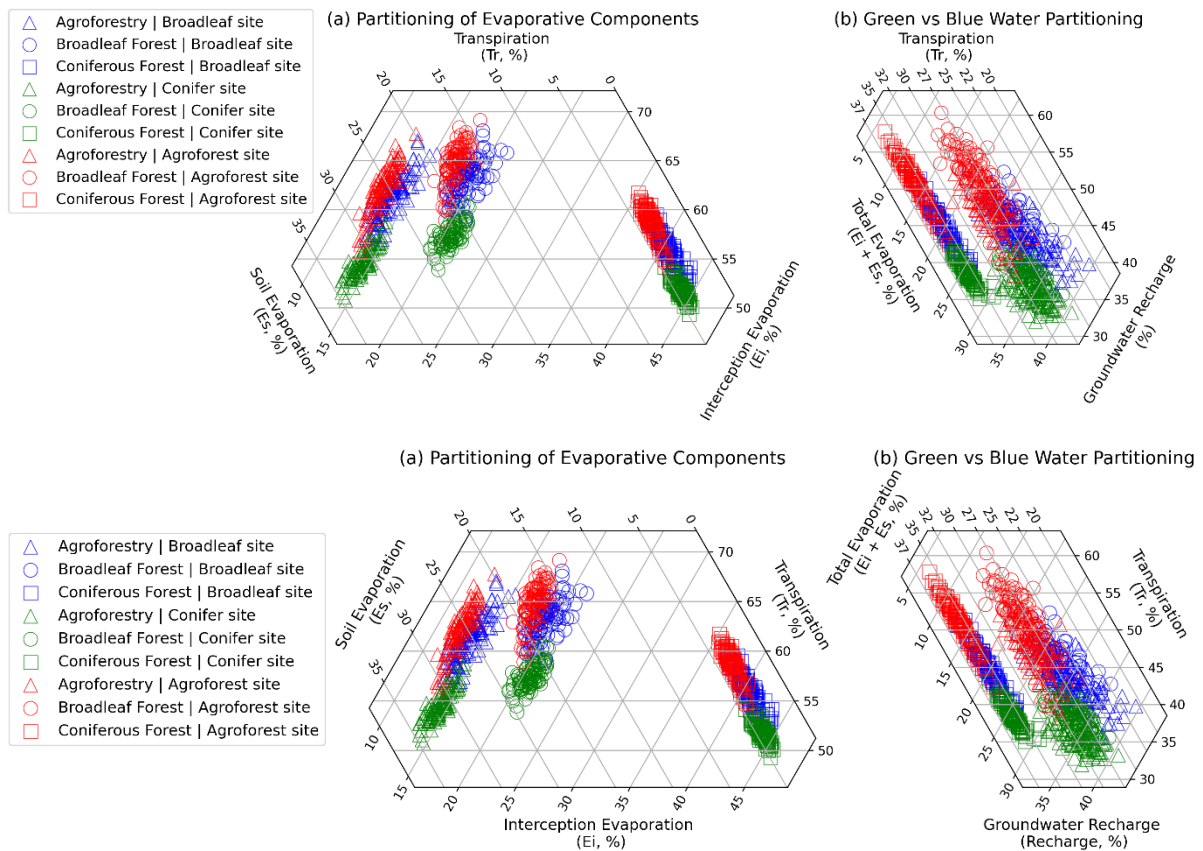
723 Figure 7 presents ternary diagrams illustrating the relative partitioning of key water flux components across three
 724 forest types based on individual simulations from the paired vegetation–site soil parameter configurations under
 725 reference canopy and rooting conditions. Transpiration predominates in all three forest types (Fig. 7a). The conifer
 726 forest exhibits a distinct pattern, characterized by the lowest soil evaporation (Es) and the highest interception
 727 evaporation (Ei) partitioning compared to broadleaf forest and agroforestry systems (Fig. 7a). In terms of green–
 728 blue water partitioning, the agroforestry system shows the largest groundwater recharge contribution (Fig. 7b).

729 Figure 7b also highlights a clear trade-off between transpiration and groundwater recharge, reflecting both
 730 equifinality among the 100 best-performing parameter sets and differences in site-specific soil properties.

731 Broadleaf and agroforestry forests display largely overlapping partitioning patterns overall, although interception
 732 evaporation and total evaporation differ notably between the two (Fig. 7a–b). Differences in soil properties also
 733 influence transpiration partitioning, following the order agroforestry site > broadleaf site > conifer site. The
 734 conifer site is characterized by coarse sandy soil with lower water retention and faster drainage, whereas the

735 agroforestry site has greater water-holding capacity, which likely contributes to the observed differences in
 736 transpiration.

737



759 Consistent with these detailed patterns, Figure 8 shows that both transpiration and evapotranspiration increase
760 with higher LAI scaling factors, while groundwater recharge decreases. Figures 8a and 8b illustrate the trade-off
761 between increased ET and reduced groundwater recharge under different forest management scenarios. ET and
762 Tr ~~transpiration and ET~~ rise rapidly at first, then slow down and transpiration even slightly decreases for conifer
763 forests due to increased interception evaporation and soil moisture limitation (Figs. 8c and 8i). This decline is not
764 observed in broadleaf or agroforestry systems, likely due to their different seasonal LAI patterns. While summer
765 LAI values for broadleaf and coniferous forests may be similar, the consistently high year-round LAI in conifers
766 can exacerbate moisture stress.

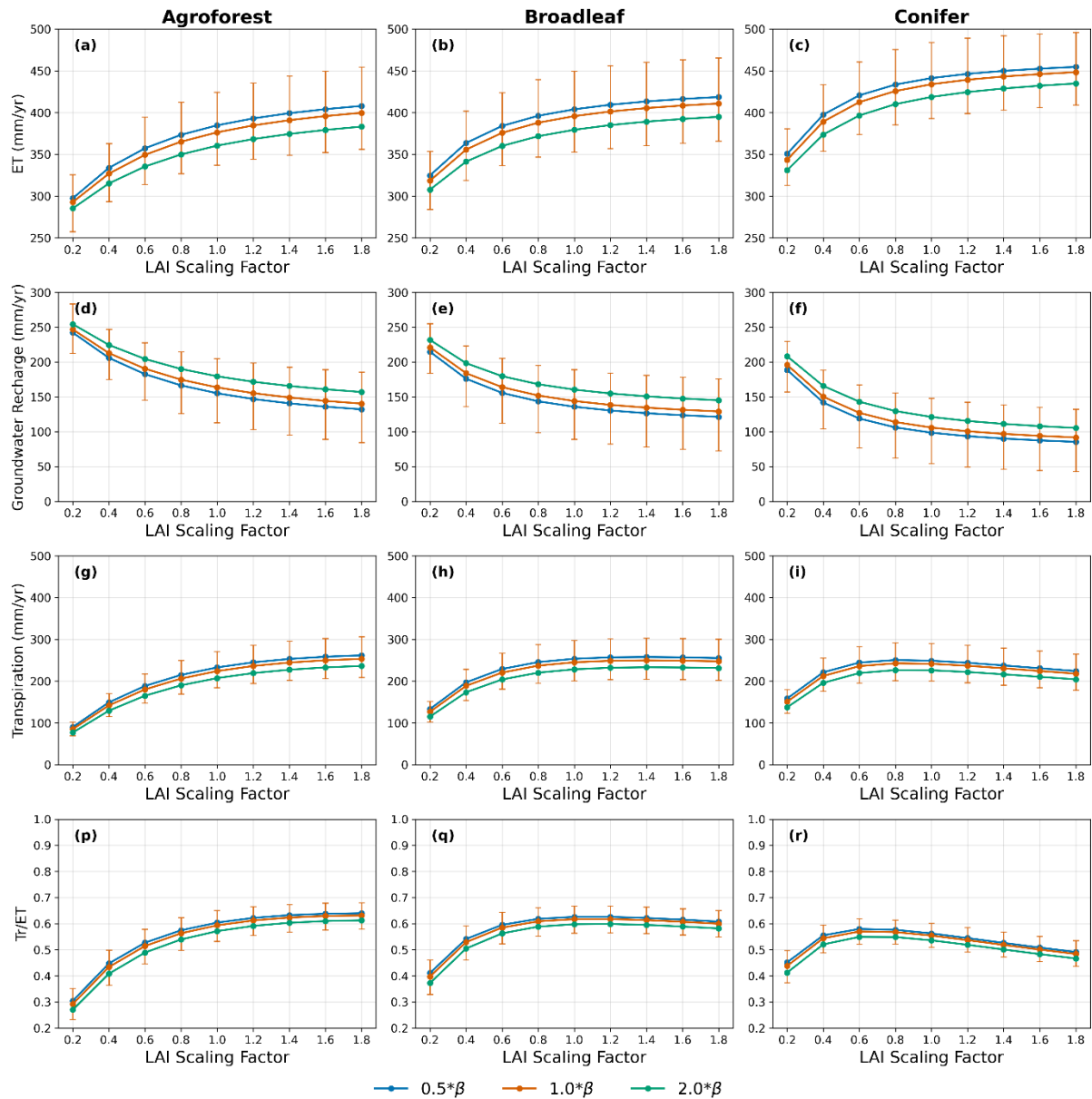
767 At higher LAI levels, transpiration decreases slightly while canopy interception evaporation increases (Fig. S11).
768 In dense coniferous stands, excessive interception and persistently dry soils limit root water uptake, reducing
769 vegetation function. This highlights a trade-off between transpiration and interception evaporation. The resulting
770 moisture limitation suggests that such high-density forests may not be sustainable under water-limited conditions,
771 as this negative feedback could constrain long-term forest growth and persistence. In addition, forests with
772 shallow-rooted trees—such as young stands—tend to transpire less, generate more groundwater recharge, and
773 exhibit lower Tr/ET ratios compared to deep-rooted forests. ~~However, even at constant LAI, transpiration declines~~
774 ~~with increasing canopy density~~ However, under high canopy density conditions, transpiration declines across
775 rooting scenarios, suggesting that this reduction is driven not only by soil moisture limitation, but also by increased
776 interception evaporation.
777 ~~, suggesting that rooting depth alone cannot compensate for moisture limitations in dense forests.~~

778

779

780

781



782
783
784
785
786
787
788

Figure 8. Annual mean ecohydrological fluxes for three forest types (Agroforest, Broadleaf, and Conifer) under varying LAI scaling factors and root depth scenarios, based on the ensemble mean of simulations derived from the paired vegetation–site soil parameter configurations (Figure 3). Panels (a)–(c) show evapotranspiration (ET), (d)–(f) show groundwater recharge, (g)–(i) show transpiration, and (p)–(r) show the ratio of transpiration to total evapotranspiration (Tr/ET). Lines represent different rooting depth scenarios (β), while vertical bars denote the 5th–95th percentile range across ensemble simulations for the baseline rooting scenario ($\beta = 1 \times \beta$).

789 4.3.3 Monthly Dynamics of Water Fluxes Responses to Forest Management Scenarios

790 Figure 9 shows monthly deviations in water balance components across forest management scenarios, based on
791 the ensemble mean of simulations derived from the paired vegetation–site soil parameter configurations (Fig. 3)
792 under reference canopy and rooting conditions (LAI scaling = 1; $\beta = 1 \times \beta$). Relative differences among forest
793 types indicate that agroforestry exhibits lower transpiration and canopy evaporation, but higher soil evaporation
794 during summer compared to broadleaf forests (Fig. 9a). They are also associated with greater groundwater
795 recharge from summer through the following winter. A shift from broadleaf to conifer forests is expected to have
796 a greater impact on the water balance than the shift from agroforest to broadleaf (Fig. 9a and 9b). Compared to
797 broadleaf forests, conifer forests exhibit higher simulated transpiration in March (Fig. 9b), driven by increased

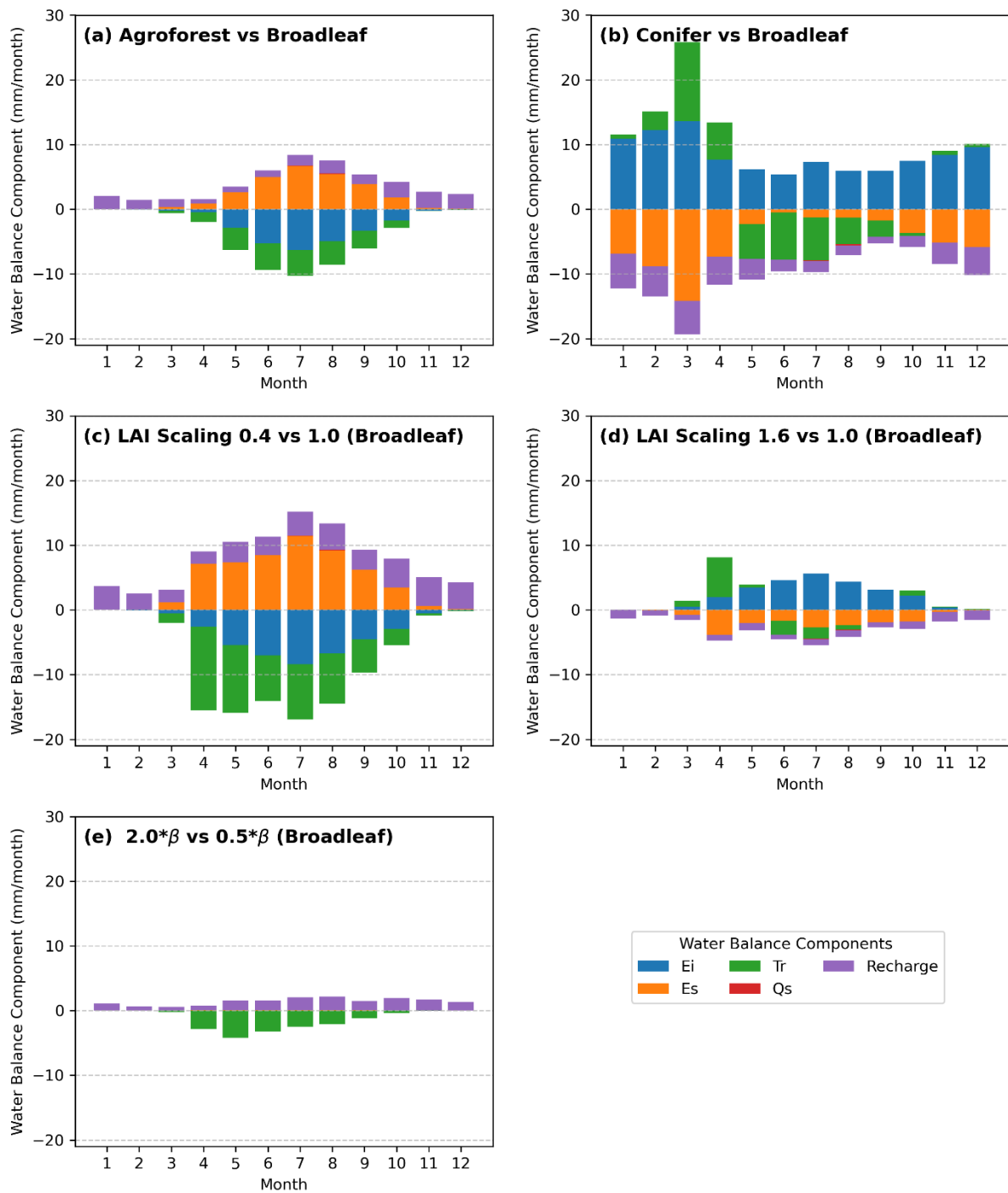
798 potential evapotranspiration and a relatively higher leaf area index (LAI) under wet soil conditions. This difference
799 diminishes as the LAI of broadleaf forests increases in spring.

800 Changes in the LAI scaling factor influence water balance components in summer, increasing transpiration and
801 canopy evaporation while reducing recharge and soil evaporation (Fig. 9c and 9d). Increasing the LAI scaling
802 factor from 0.4 to 1.0 has a greater impact than reducing it from 1.6 to 1.0, as vegetation water use responds more
803 sensitively at low LAI values but plateaus at higher values due to energy or soil moisture limitations. Altering the
804 forest root parameter (β), while using the same LAI time series, primarily affects deep-layer transpiration,
805 reducing total transpiration and increasing recharge. Other water balance components remain unchanged because
806 the LAI time series is held constant.

807 Figure 10 extends the monthly analysis by explicitly comparing wet-dry-year differences in water balance
808 responses ~~between wet and dry years~~ across forest type, canopy density, and rooting scenarios. In contrast to
809 Figure 9, which presents mean monthly deviations relative to reference conditions, and Figure 5b, which shows
810 the baseline wet-dry-year differences, Figure 10 highlights how these wet-dry contrasts ~~deviations vary among~~
811 ~~scenarios~~ differ under contrasting hydroclimatic conditions, thereby isolating drought-sensitivity effects.

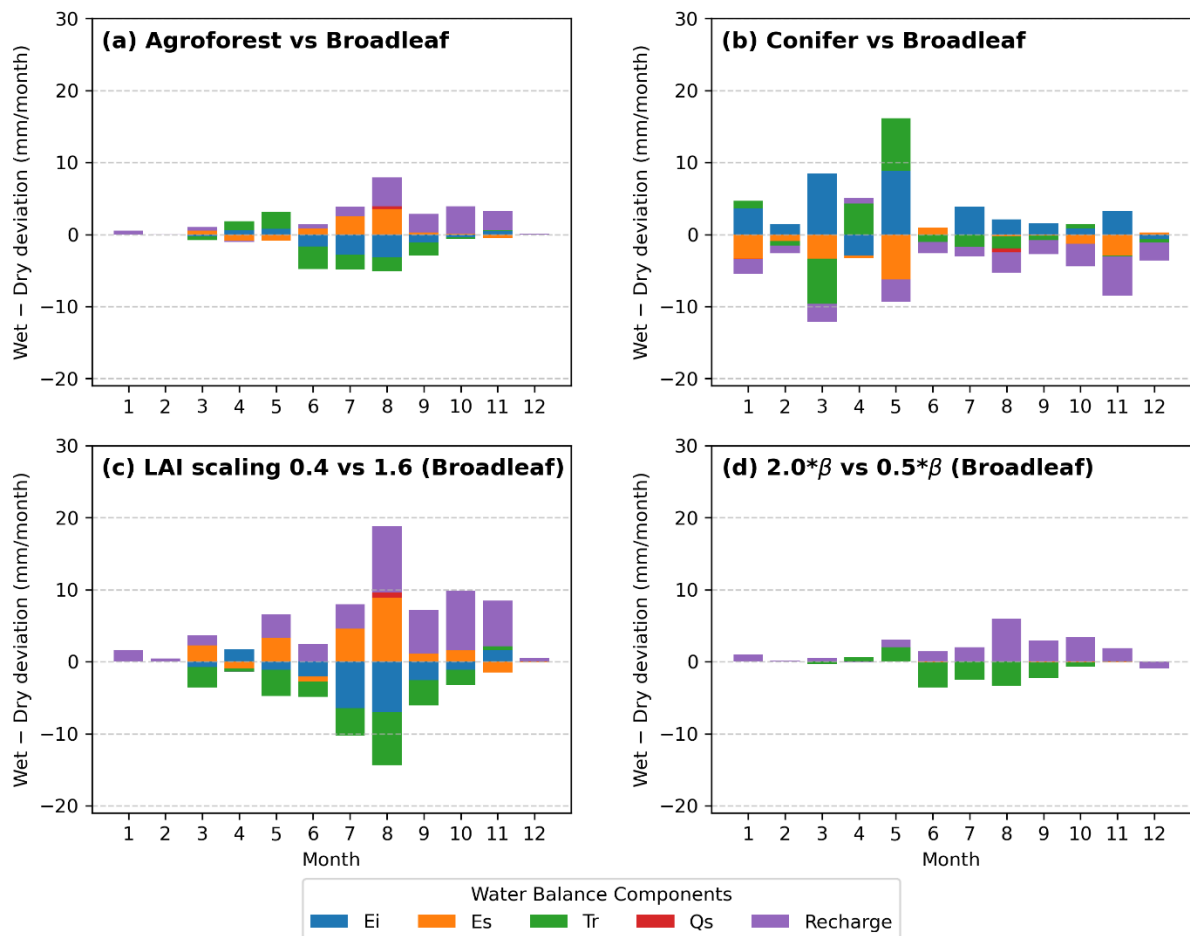
812 For agroforestry relative to broadleaf forests, hydroclimatic contrasts primarily affect groundwater recharge and
813 transpiration, with the largest wet-dry differences occurring in late summer (Fig. 10a). This indicates a more
814 buffered late-summer transpiration response in agroforestry systems under drought conditions. In contrast,
815 differences between coniferous and broadleaf forests show the largest wet-dry contrasts in transpiration during
816 May (Fig. 10b), rather than March as indicated by the mean monthly deviations in Figure 9b. This seasonal shift
817 indicates that conifer transpiration is most drought-sensitive during the later spring period, likely reflecting
818 sustained year-round transpiration and associated soil moisture drawdown in conifer forests, and highlighting
819 differences in early growing-season water-use strategies between coniferous and broadleaf forests.

820 Figures 10c and 10d show that wet-dry differences are largest in summer (August), indicating that drought
821 conditions amplify ecohydrological differences between low and high canopy density, as well as between shallow
822 and deep ~~root~~ rooting scenarios, particularly for transpiration and groundwater recharge. Overall, Figure 10
823 demonstrates that hydroclimatic extremes not only modify the magnitude of vegetation controls on water
824 partitioning but also shift their seasonal expression, with important implications for ecohydrological resilience
825 under future drought conditions.



826
 827 **Figure 9.** Monthly deviations of water balance components relative to the baseline broadleaf forest scenario, based
 828 on the ensemble mean of simulations derived from the paired vegetation–site soil parameter configurations (Fig.
 829 3) under reference canopy and rooting conditions (LAI scaling = 1; $\beta = 1 \times \beta$). Each panel illustrates the deviation
 830 of monthly water balance components from the baseline simulation, with only one parameter modified in each
 831 scenario: (a) Agroforest, (b) Conifer forest, (c) LAI scaling factor = 0.4, (d) LAI scaling factor = 1.6, and (e) Root
 832 parameter $\beta = 2.0$. Tr: transpiration, Ei: canopy evaporation, Es: soil evaporation, Qs: surface runoff, Recharge:
 833 groundwater recharge.

834



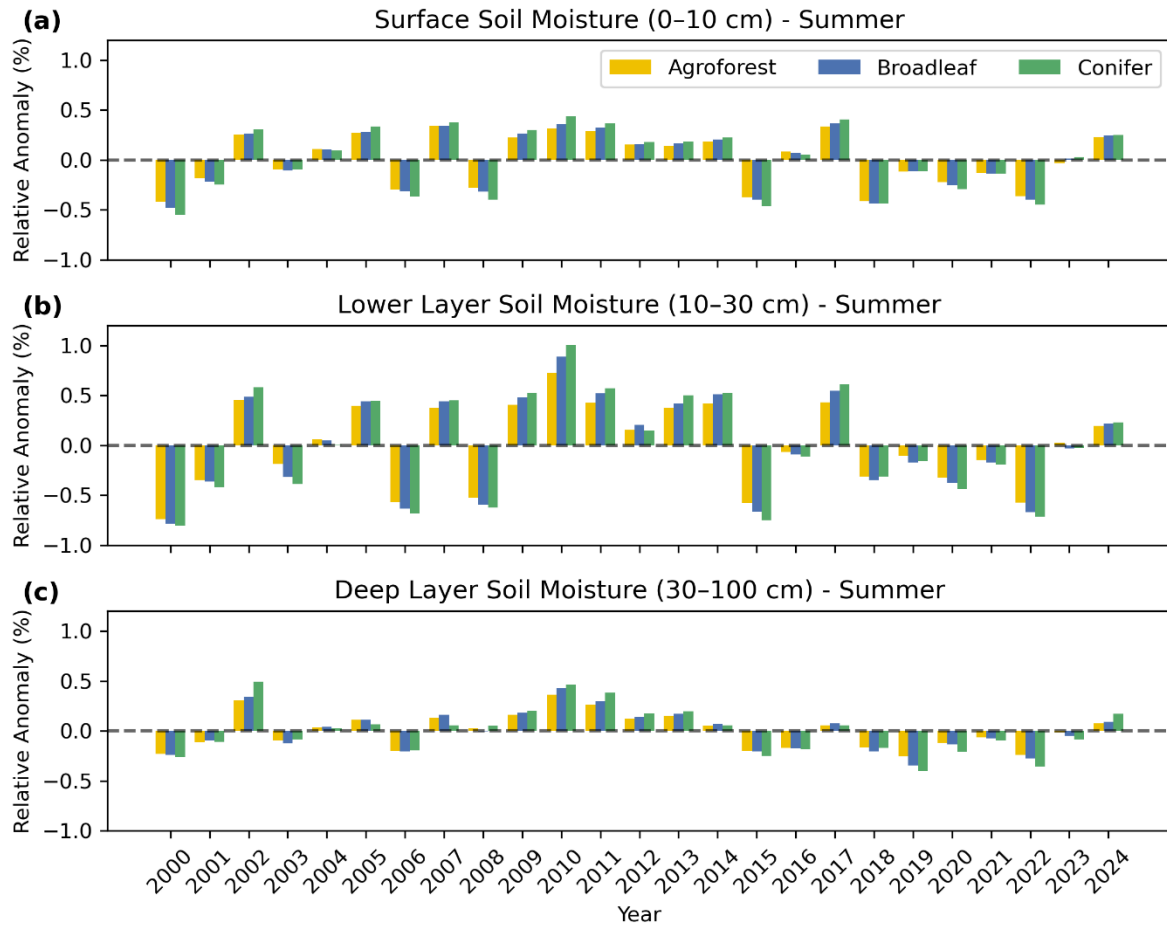
835

836 **Figure 10.** Monthly differences in water balance component deviations between wet and dry years across forest type, LAI scaling, and rooting (β) scenarios. For each panel, values show the difference between wet-year and
837 dry-year deviations of a given scenario relative to its reference scenario; positive (negative) values indicate
838 stronger (weaker) contributions during wet years. Panels show: (a) Agroforest vs. Broadleaf; (b) Conifer vs.
839 Broadleaf; (c) LAI scaling 0.4 vs. 1.6 for Broadleaf; (e) $2.0 \times \beta$ vs. $0.5 \times \beta$ for Broadleaf. Stacked bars indicate
840 contributions from interception evaporation (E_i), soil evaporation (E_s), transpiration (T_r), surface runoff (Q_s), and
841 groundwater recharge (Recharge). Wet years are 2002, 2007, 2010, and 2023; dry years are 2006, 2018, and 2022.

843 4.3.4 Soil Moisture Anomalies

844 Figure 11 shows the relative summer soil moisture anomalies across three forest types and three soil layers.
845 Anomalies are calculated as the percentage deviation from the long-term seasonal mean, enabling normalized
846 comparison across forest types and soil layers. Conifer forests exhibit the strongest soil moisture anomalies,
847 followed by broadleaf forests, while agroforests exhibit the least variability, indicating greater stability in soil
848 moisture. Furthermore, among the three soil layers, the intermediate layer (10–30 cm) consistently shows stronger
849 anomalies across all forest types, with magnitudes nearly double those of the other layers, highlighting its
850 vulnerability during summer drought. In contrast, the surface layer (0–10 cm) and deep layer (30–100 cm) exhibit
851 weaker anomalies, likely due to frequent soil moisture replenishment by summer rainfall in the surface layer and
852 either more stable moisture retention or greater water storage capacity at depth that compensates for drought
853 impacts. Negative soil moisture anomalies are more pronounced in summer than in spring, reflecting the stronger
854 seasonal drought effects and fluctuations in soil moisture (see Fig. S12). During spring, broadleaf forests and

855 agroforests display similar negative soil moisture anomalies, suggesting comparable seasonal soil moisture
 856 dynamics between these forest types.



857
 858 **Figure 11.** Relative summer (June–August) soil moisture anomalies across three soil layers: (a) surface (0–10
 859 cm), (b) lower layer (10–30 cm), and (c) deep layer (30–100 cm) for three forest types (Agroforest, Broadleaf,
 860 Conifer). Results are based on the ensemble mean of simulations derived from the paired vegetation–site soil
 861 parameter configurations (Fig. 3) under reference canopy and rooting conditions (LAI scaling = 1; $\beta = 1 \times \beta$).
 862 Bars represent deviations from the long-term mean, with positive values indicating wetter conditions and negative
 863 values indicating drier conditions.

864 **5 Discussion**

865 **5.1 Vegetation Controls on Water Partitioning under Contrasting Forest Management Scenarios**

866 Assessing the influence of different land use types on water availability is inherently challenging because of the
 867 complex interactions among vegetation, climate, and soil properties (te Wierik et al., 2021; Zhang et al., 2001).
 868 Different vegetation types have distinct water demands, and their contrasting canopy structures affect how
 869 precipitation is intercepted and partitioned into infiltration, runoff, groundwater recharge, and evapotranspiration
 870 (Brauman et al., 2010). Vegetation management practices can substantially alter these processes. Moreover, the
 871 effects of vegetation and canopy structure may vary depending on underlying soil characteristics (Geris et al.,
 872 2015). This complexity poses a significant challenge for land managers and policymakers, particularly in drought-
 873 sensitive regions experiencing increasing aridity under climate change (Orth & Destouni, 2018). In such contexts,

914 providing informed guidance on sustainable land cover choices is increasingly important for maintaining long-
915 term water availability (Estrela & Vargas, 2012). In regions where forestry has traditionally been a dominant land
916 use, shifting hydroclimatic conditions underscore the need to assess ~~the resilience of how~~ different forest types and
917 management practices affect water partitioning and drought vulnerability (Quandt et al., 2023). This requires
918 evaluating water yield across multiple temporal scales, including the effects of forest management on annual and
919 monthly water partitioning, and their implications for residual water availability—specifically streamflow
920 generation and groundwater recharge during low-flow periods (Brown et al., 2005; Neill et al., 2021).

921 Although complex, process-based ecohydrological models such as RHESSys and EcH₂O are well suited to
922 capturing detailed interactions among hydrological processes and water fluxes in data-rich research settings, their
923 broader application in forest and land management is often constrained by the availability of observation data
924 required for model forcing and calibration, as well as computational demand (Fatchi et al., 2012; Kuppel et al.,
925 2018; Tague & Band, 2004). In this study, we therefore adopt a parsimonious, tracer-aided, conceptual process-
926 based modelling approach. This was not to replace more complex models, but to provide robust and management-
927 relevant insights into the dominant vegetation-structural controls governing water partitioning under different
928 forest management scenarios. This focus is particularly relevant for Brandenburg, northeastern Germany, where
929 recent droughts have highlighted the vulnerability of traditional forest management practices dominated by Scots
930 pine plantations (Luo et al., 2024). By employing the tracer-aided ecohydrological model EcoPlot-iso, we
931 developed and applied a generic framework to quantify the long-term effects of variations in forest type, forest
932 density and root distribution on both blue and green water fluxes. The framework is based on idealized
933 monoculture forest scenarios and explicitly acknowledges that additional species-specific and process-level
934 dynamics (e.g., stomatal regulation, VPD sensitivity, drought stress strategies) are not ~~represented~~ represent and
935 remain important directions for future model development. While this study focused on idealized, homogeneous
936 vegetation scenarios (broadleaf, and conifer, ~~and agroforestry~~) for clarity and comparability, ~~EcoPlot iso can be~~
937 ~~extended to simulate mixed crop-tree systems mixed-species such as agroforestry stands could only be represented~~
938 ~~implicitly in EcoPlot-iso through aggregated plot-scale vegetation parameters, as its ecohydrological parameters~~
939 ~~are calibrated at the plot scale using a Monte Carlo approach, making it suitable for regions where diverse forest~~
940 ~~compositions are the norm. Species-specific interactions and sub-grid vegetation heterogeneity are therefore not~~
941 ~~explicitly resolved.~~ The applied LAI scaling range represents an intentionally broad, management-relevant
942 envelope for exploring canopy density effects, and scenario results should therefore be interpreted in a relative
943 rather than prescriptive sense.

944 We acknowledge that the calibration of EcoPlot-iso is subject to parameter equifinality, whereby multiple
945 parameter combinations can reproduce the observed soil moisture and isotope dynamics with similarly good
946 performance. Rather than seeking a single optimal parameter set, our calibration strategy explicitly accounts for
947 this equifinality by propagating uncertainty from the 100 best-performing simulations into all key results. The
948 scenario framework further assumes that vegetation- and soil-related parameter sets can be recombined for
949 comparative scenario analysis, without explicitly preserving parameter correlations among the calibrated
950 ensembles. This may contribute to uncertainty inflation in some flux estimates and should therefore be considered
951 when interpreting the prediction intervals. Uncertainty envelopes (5th–95th percentiles) shown in Figures 4, 6,
952 and 8 illustrate the range of annual and seasonal flux responses, enabling the magnitude of parametric uncertainty
953 to be evaluated relative to differences among forest types and management scenarios. Although parametric

954 uncertainty is non-negligible and in some cases comparable to different forest management scenarios, the main
955 findings are supported by consistent ensemble-mean responses and clear directional differences in water
956 partitioning across scenarios. Accordingly, results are interpreted in a relative and comparative sense, emphasizing
957 management-relevant trade-offs rather than absolute flux predictions.

958 In the baseline simulations for broadleaf forest, conifer forest and agroforestry at the DMC site, the estimated
959 mean annual evapotranspiration (ET) over 2000–2024 was 396, 434, and 376 mm yr⁻¹, respectively, accounting
960 for approximately 73%, 80%, and 69% of annual precipitation. These values are consistent with previous
961 modelling studies at the DMC, which reported ET fractions ranging from 68% to over 80% of annual precipitation
962 (Smith et al., 2021; Landgraf et al., 2023). Differences among studies may reflect interannual climate variability
963 and the influence of particularly dry or wet years that are not captured by short-term assessments. Differences in
964 model structure, parameterization, and input data may also contribute to the spread in reported ET values. In
965 addition, to further assess model performance using an independent data source, simulated ET was evaluated
966 against MODIS-derived ET for all land use sites in the DMC, including broadleaf forest, conifer forest,
967 agroforestry, cropland, and grassland (Fig. S8 and Table S4). Model performance was quantified using mKGE
968 metrics calculated from daily ET, providing an external validation independent of the calibration data. While
969 EcoPlot-iso tends to slightly underestimate ET relative to MODIS observations, mKGE values indicate good
970 agreement in temporal dynamics across land-use types, supporting the model’s ability to reproduce key ET
971 variability. Overall, this evaluation underscores the importance of long-term simulations and independent data-
972 based validation for capturing representative ecohydrological behavior and for assessing the impacts of forest
973 management strategies under variable climatic conditions.

974 In catchments like DMC, where evapotranspiration (ET) is high, atmospheric demand is the primary driver of root
975 water uptake, though vegetation plays a key role in regulating its impact on water availability. In Brandenburg,
976 coniferous forests have traditionally been favored on sandy soils, but modelling indicates high water use due to
977 interception losses and year-round transpiration potential (Fig. S9c). Consequently, the implications for both
978 reduced groundwater recharge and reduced forest productivity ~~have~~ encouraged landowners to explore
979 alternative land use, such as broadleaf ~~forests~~ and agroforestry. These options have the potential ~~for to~~
980 optimizing biomass productivity ~~and land use resilience while enhancing with increased~~ landscape water
981 retention, ~~and increased~~ groundwater recharge, and drought adaptation.

982

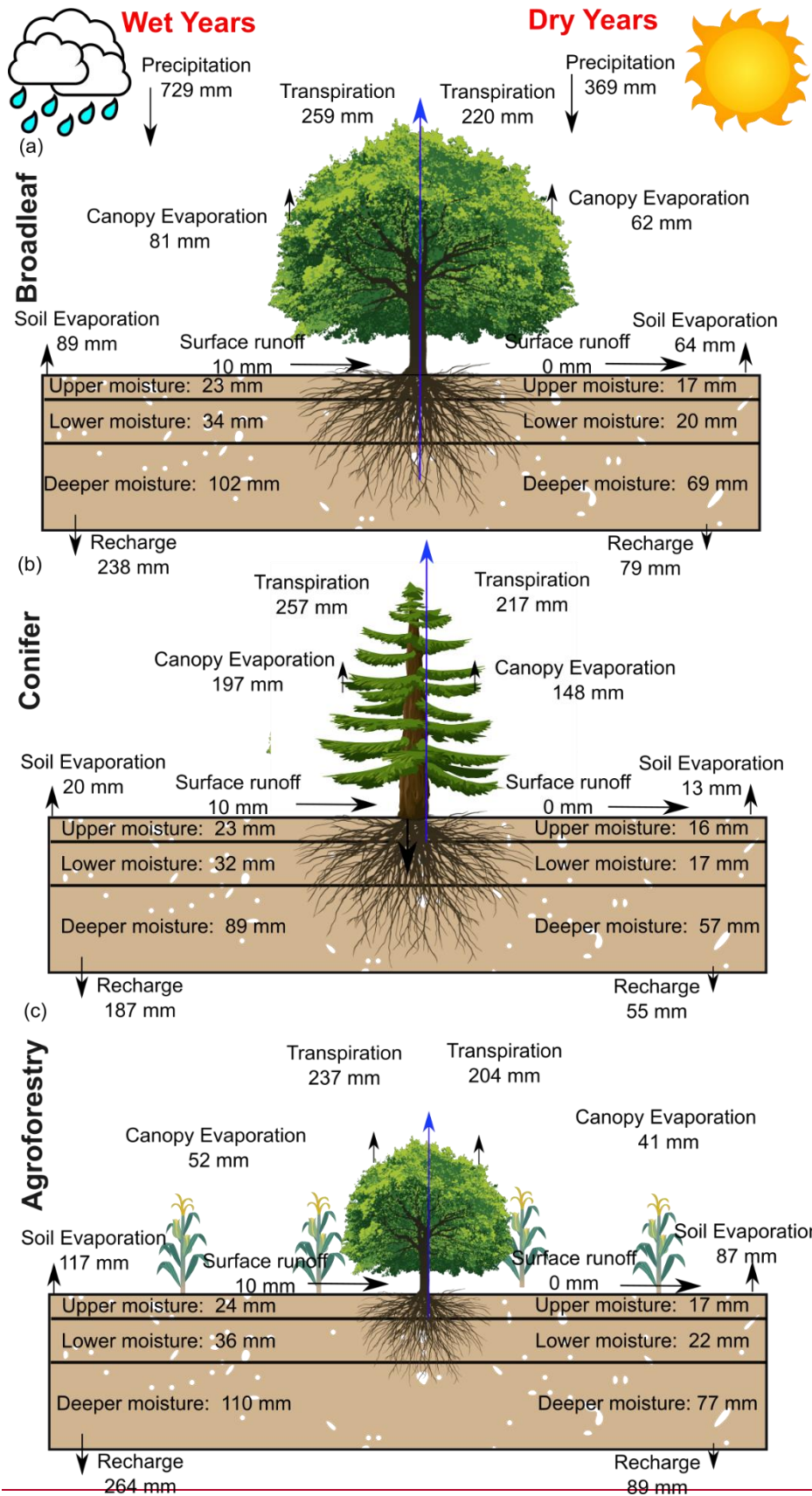
983 These results (e.g., Figs. 8 and S10) have practical applications, such as estimating the direction and magnitude
984 of the changes in evapotranspiration and water yield as a function of forest management practices, driven by
985 alterations in canopy structure and rooting depth. The modelling approach thus provides useful insights into the
986 hydrological implications of alternative canopy structures and rooting patterns for water use. Figure 12 compares
987 the mean annual partitioning of water fluxes and soil moisture across broadleaf, coniferous, and agroforest types
988 under dry and wet year conditions. It highlights how different vegetation strategies influence ecohydrological
989 resilience, with substantial differences in water partitioning observed between dry and wet years across contrasting
990 forest management scenarios. By simulating long-term water availability across ~~periods of~~ alternating wet and dry
991 conditions years, EcoPlot-iso simulations suggest that ~~mixed forests and~~ agroforestry can support enhance water

996 ~~supply-availability resilience~~ in drought-sensitive catchments by sustaining ~~both water yield and~~ groundwater
997 recharge as the dominant blue-water flux.

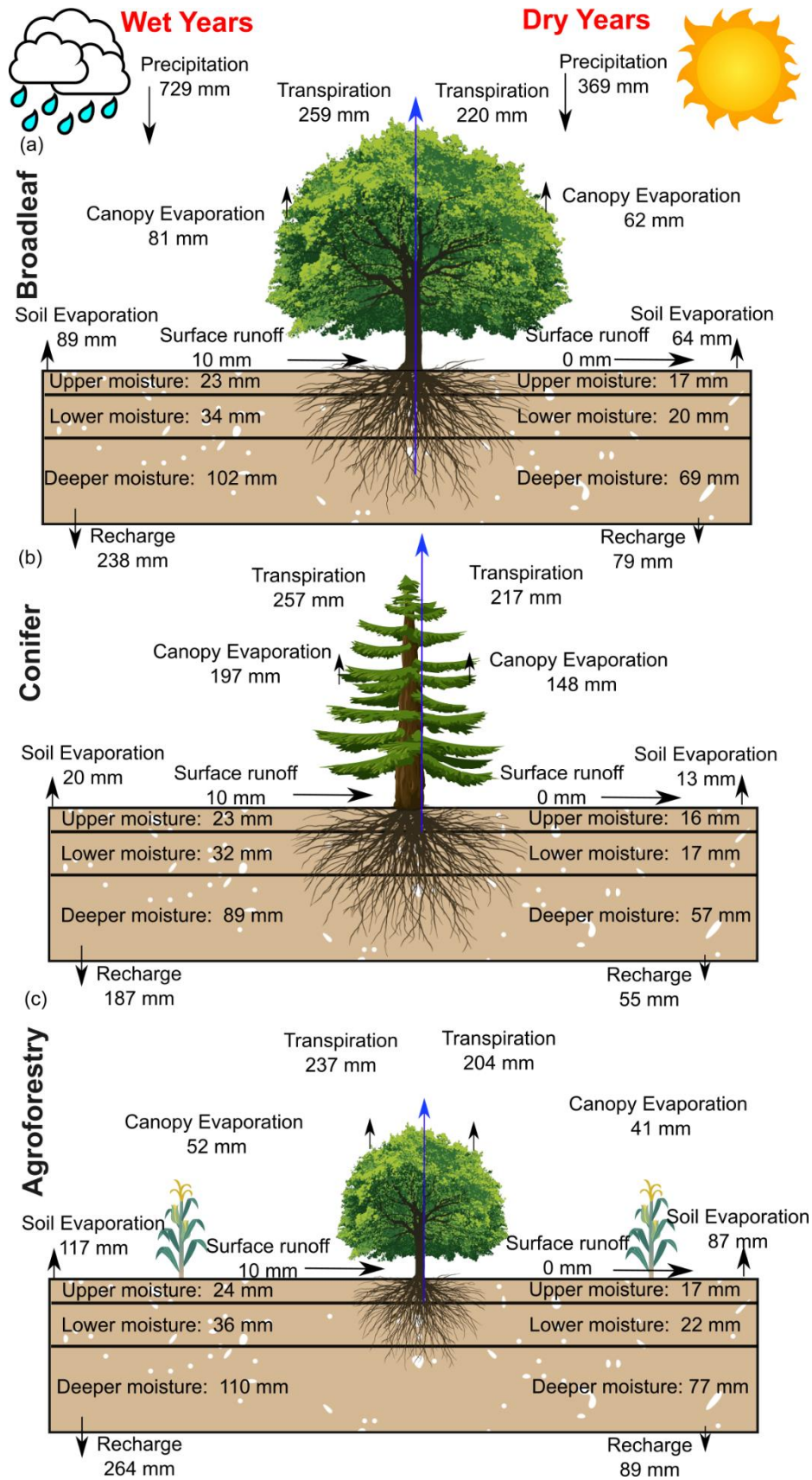
998

999

Formatted



1000



1001
1002
1003
1004

Figure 12. Comparison of mean annual water fluxes and soil moisture in the upper, lower/middle, and deeper layers for Broadleaf (a), Coniferous (b), and Agroforestry (c) forests under dry (2006, 2018, 2022) and wet (2002, 2007, 2010, 2023) year conditions.

1005 **5.2 Soil Moisture Dynamics and Root Water Uptake Processes across Forest Management Scenarios**

1006 At most of the monitoring plots in the DMC, groundwater is typically more than 3 meters below the ground surface
1007 (Ying et al., 2025). Therefore, except in older forest plots with deeply rooting trees, vegetation relies on soil
1008 moisture for root water uptake. Even for mature trees, there is evidence that most root water uptake occurs in the
1009 near-surface soil horizons, as demonstrated by Birkel et al. (2025), 20 km from the DMC. A global synthesis by
1010 Evaristo & McDonnell (2017) further supports this, indicating that ~77% of plant water uptake comes from
1011 shallow sources, with deeper groundwater use primarily in more arid regions. While hydraulic redistribution may
1012 provide deeper access for some species (Emerman & Dawson, 1996), rooting strategies are complex and highly
1013 species-specific (Demir et al., 2024). In this context, our results highlight the intermediate soil layer (10–30 cm)
1014 as the most reactive and significant for sustaining transpiration, with anomaly magnitudes nearly twice those of
1015 both the shallow (0–10 cm) and deeper (30–60 cm) layers across all forest types.

1016 In addition, seasonal comparisons revealed that summer soil moisture anomalies were more negative than those
1017 in spring for all forest types (Fig. S12). This is likely linked to higher temperatures and evapotranspiration during
1018 summer, which intensify water stress and drive seasonal variation in soil moisture availability. Forest density and
1019 rooting characteristics substantially influenced the relative magnitude of soil moisture anomalies (Figs. S13 and
1020 S14, respectively). Denser forests exhibited stronger negative anomalies during dry periods and enhanced positive
1021 anomalies in wet periods, amplifying seasonal fluctuations. For example, high-density (LAI scaling factor 1.6)
1022 conifer stands showed relative anomalies up to 25% greater than their low-density counterparts (Fig. S14). In
1023 contrast, shallow-rooted systems moderated this response, leading to more stable soil moisture dynamics. Among
1024 the management scenarios, agroforestry consistently exhibited the smallest anomalies, reflecting greater buffering
1025 capacity and higher ecohydrological resilience.

1026 The improved rooting scheme in EcoPlot-iso represents depth-dependent transpiration by dynamically linking
1027 root water uptake efficiency to soil moisture availability across three soil compartments (see Section 3.2). ~~The~~
1028 ~~implemented formulation enables transpiration demand to be partitioned across soil layers according to rooting~~
1029 ~~distribution and soil moisture availability within a parsimonious conceptual framework. Unlike models such as~~
1030 ~~RHESSys and EeH2O, which partition a prescribed total transpiration—typically derived from the energy~~
1031 ~~balance—across layers based on static root distributions, our approach allows transpiration to emerge from~~
1032 ~~potential evapotranspiration, root zone constraints, and soil moisture availability.~~ The aim was not to optimize
1033 species-specific root dynamics, but to represent the relative influence of rooting depth on water uptake and
1034 partitioning, particularly in shallow-rooted or structurally diverse systems such as young forests. While the new
1035 implementation improves the process representation of root–soil interactions, it did not result in a substantial
1036 improvement in simulated soil moisture. For shallow vegetation types such as grasslands and croplands, model
1037 performance—measured using the mKGE was similar with and without the new transpiration function (results
1038 not shown). Moreover, direct validation of the root uptake scheme remains challenging due to the lack of
1039 supporting observations, such as root distribution data, xylem water isotopes, or sap flux measurements.
1040 Addressing this issue is a clear priority for future research.

1041 These findings highlight how structurally diverse systems, such as agroforests, ~~enhance the can~~ buffering drought
1042 ~~impact~~ capacity of ecosystems by improving groundwater recharge and reducing the amplitude of soil moisture
1043 ~~fluctuations, thereby supporting greater resilience during dry periods~~ (Tetzlaff et al., 2024). Together, these

1044 insights underscore the importance of rooting depth, forest structure, and seasonal climate variability in shaping
1045 soil moisture patterns and regulating vegetation [resilience](#)[water use](#). Accounting for these factors is essential for
1046 informing adaptive forest management in drought-~~sensitive~~[prone](#) catchments like the DMC.

1047 **5.3 Advancing Tracer-Aided Ecohydrological Modelling: Challenges and Future Outlook**

1048 This study demonstrates that tracer-aided ecohydrological models, such as the isotope-aided EcoPlot-iso, can be
1049 used to effectively quantify the impact of forest management scenarios on water partitioning and ecohydrological
1050 resilience. By distinguishing between evaporation, transpiration, and subsurface water movements using stable
1051 isotopes (Soulsby et al., 2015), the model captures key hydrological responses—including evapotranspiration
1052 (ET), groundwater recharge, and soil moisture dynamics—under varying management strategies. These insights
1053 support evidence-based decision-making in drought-sensitive landscapes.

1054 Despite these advances, several challenges remain. Conducted in a 66 km² mid-sized basin, this study did not
1055 include land use change induced atmospheric feedbacks—such as changes in albedo, radiative balance, or rainfall
1056 patterns—which are less critical at this scale but become important in larger-scale modeling (Ellison et al., 2012;
1057 Filoso et al., 2017). Moreover, this study applied a multi-objective calibration approach, combined with Monte
1058 Carlo sampling, that equally weighted isotopic and soil moisture data. However, further investigation is needed
1059 [into](#) how these observational constraints are balanced and interpreted. Recent advances—such as the
1060 DREAM(LoAX) framework (Wu et al., 2025)—demonstrate how simultaneous calibration and diagnostic
1061 analysis under the equifinality thesis can improve parameter identifiability, model robustness, and process
1062 understanding in tracer-aided ecohydrological models.

1063 While this study used $\delta^2\text{H}$ to constrain evaporative fractionation given, the combined use of $\delta^{18}\text{O}$ and $\delta^2\text{H}$ (or d-
1064 excess) may help improve the separation of evaporation effects and mixing processes (e.g. Penna et al., 2018)
1065 though this was beyond the scope of this paper. Many recent studies have used isotopic data to investigate root
1066 water uptake patterns, revealing how tree species, soil properties, and spatial water availability shape plant water
1067 use strategies (Demir et al., 2024; Rothfuss & Javaux, 2017). Integrating tracer-aided models with soil and xylem
1068 water isotope data offers a promising path to improving the representation of root water uptake, which is often
1069 simplified in current modelling approaches (Birkel et al., 2025). Improving root uptake representation requires
1070 consideration of species-specific traits and local soil-water conditions. However, the practical application of such
1071 improvements is limited by the scarcity of soil and xylem water isotope data, which are essential for constraining
1072 root water uptake dynamics but remain rare due to the labor-intensive and technically demanding nature of field
1073 sampling and laboratory analysis (Landgraf et al., 2022; Sprenger et al., 2017). This scarcity hinders the spatial
1074 and temporal resolution of observational data, limiting our ability to refine root water uptake processes in tracer-
1075 aided models.

1076 Upscaling from plot to landscape level remains complex due to spatial heterogeneity in vegetation, soils, and
1077 topography. Addressing this requires spatially distributed modeling frameworks that can explicitly capture
1078 heterogeneity in ecohydrological processes across different landscape units (Kuppel et al., 2018; van Huijgevoort
1079 et al., 2016). Enhanced integration with remote sensing techniques can also help address these scaling limitations
1080 by providing spatially continuous data on vegetation dynamics, soil moisture, and ET (Yang et al., 2023).
1081 Incorporating ET observations, for instance, could strengthen model interpretation of flux dynamics. Currently,

1082 key processes such as lateral subsurface flows and upward capillary fluxes are not explicitly represented in the
1083 EcoPlot-iso model. Including these components, along with improved representation of groundwater-surface
1084 water interactions, could improve simulations of hydrological water-connectivity and water storage
1085 dynamics~~resilience~~.

1086 It is important to note that the scenario framework presented here is intentionally exploratory and management-
1087 oriented, rather than species-specific. While EcoPlot-iso captures key controls on water partitioning through
1088 canopy structure, soil moisture dynamics, and tracer-based separation of fluxes, additional physiological traits—
1089 such as stomatal regulation, vapor pressure deficit (VPD) sensitivity, and species-specific drought stress
1090 strategies—are not explicitly represented. These processes are known to influence transpiration dynamics and
1091 vegetation responses to drought, and their inclusion represents an important direction for future model
1092 development. Accordingly, the results of this study are interpreted in a relative sense, emphasizing comparative
1093 responses and management-relevant trade-offs rather than absolute or species-level predictions.

1094 **6 Conclusion and Outlook**

1095 The tracer-aided ecohydrological model EcoPlot-iso was applied to quantify how alternative forest management
1096 scenarios influence long-term water partitioning and ecohydrological resilience in the drought-sensitive
1097 Demnitzer Millcreek catchment (DMC), northeastern Germany. Baseline simulations for the period 2000–2024
1098 were established at three forest sites (broadleaf forest, conifer forest, and agroforestry) and successfully
1099 reproduced observed soil moisture and soil water isotope ($\delta^2\text{H}$) dynamics through a multi-criteria calibration
1100 approach. A key development in this study was the integration of a depth-dependent root water uptake function,
1101 which enable the representation of transpiration across soil layers associated with contrasting rooting distributions
1102 and stand ages. Building on these baseline simulations, a generic scenario framework was applied to
1103 systematically assess the effects of forest type, forest density, and rooting characteristics on evapotranspiration,
1104 groundwater recharge, and soil moisture dynamics under contrasting dry and wet climatic conditions.

1105 The results revealed clear trade-offs between evapotranspiration (ET) and groundwater recharge across different
1106 forest management scenarios. On average, conifer forest exhibited higher ET, approximately 7–11% greater than
1107 broadleaf forest and agroforestry, accompanied by reduced groundwater recharge, particularly during low-flow
1108 periods. In contrast, agroforestry buffered drought stress, maintained lower soil moisture variability, and enhanced
1109 groundwater recharge. Conifers showed the strongest soil moisture anomalies, indicating greater drought
1110 sensitivity, while agroforests exhibited the most stable soil water storage. The intermediate soil layer (10–30 cm)
1111 was identified as the most responsive zone, consistently exhibiting the largest anomalies due to its role as the
1112 dominant root water uptake region supporting transpiration.

1113 Beyond advancing process understanding, this study provided a practical and transferable framework for land
1114 management. By incorporating key controls such as canopy properties and root distribution, EcoPlot-iso facilitates
1115 an accessible means of assessing long-term land management impacts on landscape ecohydrology. The
1116 visualization and decision-support framework developed here offers a transparent, scenario-based platform for
1117 evaluating forest management strategies in climate-sensitive regions. These tools are well-suited for informing
1118 resilient land use planning under increasing climate variability.

1119 Looking ahead, future research could usefully aim to incorporate additional isotopic tracers—such as deeper soil
1120 water (> 1 m), groundwater, and xylem water isotopes—to further constrain root water uptake functions and
1121 capture their variability across species and hydroclimatic conditions. The integration of high-resolution remote
1122 sensing data—particularly LiDAR for detailed characterization of forest structure—will enhance model
1123 parameterization and improve the spatial representation of heterogeneity in canopy height, leaf area distribution,
1124 and forest density. Advancing the EcoPlot-iso framework to incorporate lateral subsurface flows, groundwater
1125 dynamics, and coupled land–atmosphere feedbacks will support broader applications, including the assessment of
1126 large-scale land use change. Collectively, these developments will enhance model robustness and enable more
1127 informed, resilient land and water management strategies under a warming climate.

1128 **Code and data availability**

1129 The data and code that support the findings of this study are available from the corresponding author upon
1130 reasonable request.

1131 **Author contribution**

1132 CJ contributed to the methodology, software development, formal analysis, investigation, visualization, and
1133 writing of the original draft. DT contributed to conceptualization, investigation, data curation, validation,
1134 resources, project administration, and funding acquisition. SW contributed to methodology, investigation and data
1135 curation. CB contributed to software, methodology, and resources. HL contributed to investigation, visualization
1136 and validation. CS contributed to conceptualization, methodology, validation, investigation. All authors
1137 contributed to writing – review and editing.

1138 **Competing interests**

1139 The authors declare that they have no conflict of interest.

1140 **Acknowledgements**

1141 Tetzlaff's contributions were partly funded through the WETSCAPES2.0 project (DFG TRR410/1 2025). Tetzlaff
1142 also received funding from the "Wasserressourcenpreis 2024" awarded by the Rüdiger Kurt Bode-Foundation.
1143 Contributions from Soulsby were supported by Leibnitz Association Germany in the project Wetland Restoration
1144 in Peatlands. Laudon was funded by KAW 2018.0259 and 2023.0245, and Soulsby was also funded as an
1145 International KSLA Guest Professor at SLU by the Wallenberg Foundation (WP2023-0001). Birkel would like to
1146 thank the IGB for generously supporting him with a senior fellowship and the UCR for a sabbatical license. We
1147 extend our appreciation to Benedikt Boesel and the team from the Finck Foundation (www.finck-stiftung.org) for
1148 their collaborative support and for granting access to study sites. The authors are very grateful for the constructive
1149 comments provided by the Editor, Prof. Dr. Anke Hildebrandt, and two anonymous reviewers.

1150 **Reference**

- 1151 Ault, T. R. (2020). On the essentials of drought in a changing climate. In *Science* (Vol. 368, Number 6488).
1152 <https://doi.org/10.1126/science.aaz5492>
- 1153 Birkel, C., Arciniega-Esparza, S., Maneta, M. P., Boll, J., Stevenson, J. L., Benegas-Negri, L., Tetzlaff, D., &
1154 Soulsby, C. (2024). Importance of measured transpiration fluxes for modelled ecohydrological partitioning
1155 in a tropical agroforestry system. *Agricultural and Forest Meteorology*, 346.
1156 <https://doi.org/10.1016/j.agrformet.2023.109870>
- 1157 Birkel, C., Tetzlaff, D., Ring, A. M., & Soulsby, C. (2025). Does high resolution in situ xylem and atmospheric
1158 vapor isotope data help improve modeled estimates of ecohydrological partitioning? *Agricultural and*
1159 *Forest Meteorology*, 365. <https://doi.org/10.1016/j.agrformet.2025.110467>
- 1160 Bonan, G. B. (2008). Forests and climate change: Forcings, feedbacks, and the climate benefits of forests. In
1161 *Science* (Vol. 320, Number 5882). <https://doi.org/10.1126/science.1155121>
- 1162 Bosch, J. M., & Hewlett, J. D. (1982). A REVIEW OF CATCHMENT EXPERIMENTS TO DETERMINE THE
1163 EFFECT OF VEGETATION CHANGES ON WATER YIELD AND EVAPOTRANSPIRATION. In
1164 *Journal of Hydrology* (Vol. 55).
- 1165 Brauman, K. A., Freyberg, D. L., & Daily, G. C. (2010). Forest structure influences on rainfall partitioning and
1166 cloud interception: A comparison of native forest sites in Kona, Hawai'i. *Agricultural and Forest*
1167 *Meteorology*, 150(2). <https://doi.org/10.1016/j.agrformet.2009.11.011>
- 1168 Brown, A. E., Western, A. W., McMahon, T. A., & Zhang, L. (2013). Impact of forest cover changes on annual
1169 streamflow and flow duration curves. *Journal of Hydrology*, 483.
1170 <https://doi.org/10.1016/j.jhydrol.2012.12.031>
- 1171 Brown, A. E., Zhang, L., McMahon, T. A., Western, A. W., & Vertessy, R. A. (2005). A review of paired
1172 catchment studies for determining changes in water yield resulting from alterations in vegetation. *Journal*
1173 *of Hydrology*, 310(1–4), 28–61. <https://doi.org/10.1016/j.jhydrol.2004.12.010>
- 1174 Calder, I. R. (1998). Water use by forests, limits and controls. *Tree Physiology*, 18(8–9).
1175 <https://doi.org/10.1093/treephys/18.8-9.625>
- 1176 Demir, G., Guswa, A. J., Filipzik, J., Metzger, J. C., Römermann, C., & Hildebrandt, A. (2024). Root water uptake
1177 patterns are controlled by tree species interactions and soil water variability. *Hydrology and Earth System*
1178 *Sciences*, 28(6), 1441–1461. <https://doi.org/10.5194/hess-28-1441-2024>
- 1179 Douinot, A., Tetzlaff, D., Maneta, M., Kuppel, S., Schulte-Bisping, H., & Soulsby, C. (2019). Ecohydrological
1180 modelling with ECH2O-iso to quantify forest and grassland effects on water partitioning and flux ages.
1181 *Hydrological Processes*, 33(16), 2174–2191. <https://doi.org/10.1002/hyp.13480>
- 1182 Dubbert, M., Couvreur, V., Kübert, A., & Werner, C. (2023). Plant water uptake modelling: added value of cross-
1183 disciplinary approaches. In *Plant Biology* (Vol. 25, Number 1). <https://doi.org/10.1111/plb.13478>
- 1184 Ellison, D., Futter, M. N., & Bishop, K. (2012). On the forest cover-water yield debate: From demand- to supply-
1185 side thinking. In *Global Change Biology* (Vol. 18, Number 3). [https://doi.org/10.1111/j.1365-](https://doi.org/10.1111/j.1365-2486.2011.02589.x)
1186 [2486.2011.02589.x](https://doi.org/10.1111/j.1365-2486.2011.02589.x)
- 1187 Emerman, S. H., & Dawson, T. E. (1996). Hydraulic lift and its influence on the water content of the rhizosphere:
1188 An example from sugar maple, *Acer saccharum*. *Oecologia*, 108(2). <https://doi.org/10.1007/BF00334651>
- 1189 Estrela, T., & Vargas, E. (2012). Drought Management Plans in the European Union. The Case of Spain. In *Water*
1190 *Resources Management* (Vol. 26, Number 6). <https://doi.org/10.1007/s11269-011-9971-2>
- 1191 Evaristo, J., & McDonnell, J. J. (2017). Prevalence and magnitude of groundwater use by vegetation: A global
1192 stable isotope meta-analysis. *Scientific Reports*, 7. <https://doi.org/10.1038/srep44110>

- 1193 Falkenmark, M., & Rockström, J. (2006). The New Blue and Green Water Paradigm: Breaking New Ground for
 1194 Water Resources Planning and Management. *Journal of Water Resources Planning and Management*,
 1195 132(3). [https://doi.org/10.1061/\(asce\)0733-9496\(2006\)132:3\(129\)](https://doi.org/10.1061/(asce)0733-9496(2006)132:3(129))
- 1196 Fatichi, S., Ivanov, V. Y., & Caporali, E. (2012). A mechanistic ecohydrological model to investigate complex
 1197 interactions in cold and warm water-controlled environments: 1. Theoretical framework and plot-scale
 1198 analysis. *Journal of Advances in Modeling Earth Systems*, 4(5). <https://doi.org/10.1029/2011MS000086>
- 1199 Filoso, S., Bezerra, M. O., Weiss, K. C. B., & Palmer, M. A. (2017). Impacts of forest restoration on water yield:
 1200 A systematic review. In *PLoS ONE* (Vol. 12, Number 8). <https://doi.org/10.1371/journal.pone.0183210>
- 1201 Gelbrecht, J., Driescher, E., Lademann, H., Schönfelder, J., & Exner, H.-J. (1996). Diffuse nutrient impact on
 1202 surface water bodies and its abatement by restoration measures in a small catchment area in North-East
 1203 Germany. *Water Science and Technology*, 33(4–5). <https://doi.org/10.2166/wst.1996.0501>
- 1204 Gelbrecht, J., Lengsfeld, H., Pöthig, R., & Opitz, D. (2005). Temporal and spatial variation of phosphorus input,
 1205 retention and loss in a small catchment of NE Germany. *Journal of Hydrology*, 304(1–4), 151–165.
 1206 <https://doi.org/10.1016/j.jhydrol.2004.07.028>
- 1207 Geris, J., Tetzlaff, D., McDonnell, J., & Soulsby, C. (2015). The relative role of soil type and tree cover on water
 1208 storage and transmission in northern headwater catchments. *Hydrological Processes*, 29(7).
 1209 <https://doi.org/10.1002/hyp.10289>
- 1210 Guswa, A. J., Tetzlaff, D., Selker, J. S., Carlyle-Moses, D. E., Boyer, E. W., Bruen, M., Cayuela, C., Creed, I. F.,
 1211 van de Giesen, N., Grasso, D., Hannah, D. M., Hudson, J. E., Hudson, S. A., Iida, S., Jackson, R. B., Katul,
 1212 G. G., Kumagai, T., Llorens, P., Lopes Ribeiro, F., ... Levia, D. F. (2020). Advancing ecohydrology in the
 1213 21st century: A convergence of opportunities. In *Ecohydrology* (Vol. 13, Number 4). John Wiley and Sons
 1214 Ltd. <https://doi.org/10.1002/eco.2208>
- 1215 Hersbach, H., Bell, B., Berrisford, P., Hirahara, S., Horányi, A., Muñoz-Sabater, J., Nicolas, J., Peubey, C., Radu,
 1216 R., Schepers, D., Simmons, A., Soci, C., Abdalla, S., Abellan, X., Balsamo, G., Bechtold, P., Biavati, G.,
 1217 Bidlot, J., Bonavita, M., ... Thépaut, J.-N. (2020). The ERA5 global reanalysis. *Quarterly Journal of the*
 1218 *Royal Meteorological Society*, 146(730), 1999–2049. <https://doi.org/https://doi.org/10.1002/qj.3803>
- 1219 Hibbert, A. R. (1967). Forest Treatment Effects on Water Yield. *International Symposium For Hydrology*.
- 1220 Huntington, T. G. (2006). Evidence for intensification of the global water cycle: Review and synthesis. *Journal*
 1221 *of Hydrology*, 319(1–4), 83–95. <https://doi.org/10.1016/j.jhydrol.2005.07.003>
- 1222 Kleine, L., Tetzlaff, D., Smith, A., Dubbert, M., & Soulsby, C. (2021). Modelling ecohydrological feedbacks in
 1223 forest and grassland plots under a prolonged drought anomaly in Central Europe 2018–2020. *Hydrological*
 1224 *Processes*, 35(8). <https://doi.org/10.1002/hyp.14325>
- 1225 Kling, H., Fuchs, M., & Paulin, M. (2012). Runoff conditions in the upper Danube basin under an ensemble of
 1226 climate change scenarios. *Journal of Hydrology*, 424–425. <https://doi.org/10.1016/j.jhydrol.2012.01.011>
- 1227 Knighton, J., Kuppel, S., Smith, A., Soulsby, C., Sprenger, M., & Tetzlaff, D. (2020). Using isotopes to
 1228 incorporate tree water storage and mixing dynamics into a distributed ecohydrologic modelling framework.
 1229 *Ecohydrology*, 13(3). <https://doi.org/10.1002/eco.2201>
- 1230 Knighton, J., Sanchez-Martinez, P., & Anderegg, L. (2024). A global dataset of tree hydraulic and structural traits
 1231 imputed from phylogenetic relationships. *Scientific Data*, 11(1). <https://doi.org/10.1038/s41597-024-04254-4>
- 1233 Kool, D., Agam, N., Lazarovitch, N., Heitman, J. L., Sauer, T. J., & Ben-Gal, A. (2014). A review of approaches
 1234 for evapotranspiration partitioning. In *Agricultural and Forest Meteorology* (Vol. 184).
 1235 <https://doi.org/10.1016/j.agrformet.2013.09.003>
- 1236 Kumar, R., Shankar, V., & Jat, M. K. (2015). Evaluation of root water uptake models - A review. In *ISH Journal*
 1237 *of Hydraulic Engineering* (Vol. 21, Number 2). <https://doi.org/10.1080/09715010.2014.981955>

- 1238 Kuppel, S., Tetzlaff, D., Maneta, M. P., & Soulsby, C. (2018). ECH2O-iso 1.0: Water isotopes and age tracking
1239 in a process-based, distributed ecohydrological model. *Geoscientific Model Development*, *11*(7), 3045–3069.
1240 <https://doi.org/10.5194/gmd-11-3045-2018>
- 1241 Landgraf, J., Tetzlaff, D., Birkel, C., Stevenson, J. L., & Soulsby, C. (2023). Assessing land use effects on
1242 ecohydrological partitioning in the critical zone through isotope-aided modelling. *Earth Surface Processes
1243 and Landforms*, *48*(15), 3199–3219. <https://doi.org/10.1002/esp.5691>
- 1244 Landgraf, J., Tetzlaff, D., Wu, S., Freymüller, J., & Soulsby, C. (2022). Using stable water isotopes to understand
1245 ecohydrological partitioning under contrasting land uses in a drought-sensitive rural, lowland catchment.
1246 *Hydrological Processes*, *36*(12). <https://doi.org/10.1002/hyp.14779>
- 1247 Luo, S., Tetzlaff, D., Smith, A., & Soulsby, C. (2024). Assessing impacts of alternative land use strategies on
1248 water partitioning, storage and ages in drought-sensitive lowland catchments using tracer-aided
1249 ecohydrological modelling. *Hydrological Processes*, *38*(4). <https://doi.org/10.1002/hyp.15126>
- 1250 Mahmood, R., Pielke, R. A., Hubbard, K. G., Niyogi, D., Dirmeyer, P. A., McAlpine, C., Carleton, A. M., Hale,
1251 R., Gameda, S., Beltrán-Przekurat, A., Baker, B., Mcnider, R., Legates, D. R., Shepherd, M., Du, J., Blanken,
1252 P. D., Frauenfeld, O. W., Nair, U. S., & Fall, S. (2014). Land cover changes and their biogeophysical effects
1253 on climate. *International Journal of Climatology*, *34*(4). <https://doi.org/10.1002/joc.3736>
- 1254 McKay, M. D., Beckman, R. J., & Conover, W. J. (1979). Comparison of three methods for selecting values of
1255 input variables in the analysis of output from a computer code. *Technometrics*, *21*(2).
1256 <https://doi.org/10.1080/00401706.1979.10489755>
- 1257 Neill, A. J., Birkel, C., Maneta, M. P., Tetzlaff, D., & Soulsby, C. (2021). Structural changes to forests during
1258 regeneration affect water flux partitioning, water ages and hydrological connectivity: Insights from tracer-
1259 aided ecohydrological modelling. *Hydrology and Earth System Sciences*, *25*(9), 4861–4886.
1260 <https://doi.org/10.5194/hess-25-4861-2021>
- 1261 Orth, R., & Destouni, G. (2018). Drought reduces blue-water fluxes more strongly than green-water fluxes in
1262 Europe. *Nature Communications*, *9*(1). <https://doi.org/10.1038/s41467-018-06013-7>
- 1263 Penna, D., Hopp, L., Scandellari, F., Allen, S. T., Benettin, P., Beyer, M., Geris, J., Klaus, J., Marshall, J. D.,
1264 Schwendenmann, L., Volkmann, T. H. M., Von Freyberg, J., Amin, A., Ceperley, N., Engel, M., Frentress,
1265 J., Giambastiani, Y., McDonnell, J. J., Zuecco, G., ... Kirchner, J. W. (2018). Ideas and perspectives:
1266 Tracing terrestrial ecosystem water fluxes using hydrogen and oxygen stable isotopes - Challenges and
1267 opportunities from an interdisciplinary perspective. *Biogeosciences*, *15*(21). <https://doi.org/10.5194/bg-15-6399-2018>
- 1269 Pielke, R. A., Pitman, A., Niyogi, D., Mahmood, R., McAlpine, C., Hossain, F., Goldewijk, K. K., Nair, U., Betts,
1270 R., Fall, S., Reichstein, M., Kabat, P., & de Noblet, N. (2011). Land use/land cover changes and climate:
1271 Modeling analysis and observational evidence. In *Wiley Interdisciplinary Reviews: Climate Change* (Vol.
1272 2, Number 6). <https://doi.org/10.1002/wcc.144>
- 1273 Quandt, A., Neufeldt, H., & Gorman, K. (2023). Climate change adaptation through agroforestry: opportunities
1274 and gaps. In *Current Opinion in Environmental Sustainability* (Vol. 60).
1275 <https://doi.org/10.1016/j.cosust.2022.101244>
- 1276 Ricci, G. F., De Girolamo, A. M., & Gentile, F. (2020). Modeling the Effect of Different Management Practices
1277 for Soil Erosion Control in a Mediterranean Watershed. *Lecture Notes in Civil Engineering*, *67*(June), 125–
1278 132. https://doi.org/10.1007/978-3-030-39299-4_14
- 1279 Rothfuss, Y., & Javaux, M. (2017). Reviews and syntheses: Isotopic approaches to quantify root water uptake: A
1280 review and comparison of methods. *Biogeosciences*, *14*(8). <https://doi.org/10.5194/bg-14-2199-2017>
- 1281 Shen, H., Tolson, B. A., & Mai, J. (2022). Time to Update the Split-Sample Approach in Hydrological Model
1282 Calibration. *Water Resources Research*, *58*(3). <https://doi.org/10.1029/2021WR031523>

- 1283 Smith, A., Tetzlaff, D., Gelbrecht, J., Kleine, L., & Soulsby, C. (2020). Riparian wetland rehabilitation and beaver
1284 re-colonization impacts on hydrological processes and water quality in a lowland agricultural catchment.
1285 *Science of the Total Environment*, 699. <https://doi.org/10.1016/j.scitotenv.2019.134302>
- 1286 Smith, A., Tetzlaff, D., Kleine, L., Maneta, M., & Soulsby, C. (2021). Quantifying the effects of land use and
1287 model scale on water partitioning and water ages using tracer-aided ecohydrological models. *Hydrology
1288 and Earth System Sciences*, 25(4), 2239–2259. <https://doi.org/10.5194/hess-25-2239-2021>
- 1289 Soulsby, C., Birkel, C., Geris, J., Dick, J., Tunaley, C., & Tetzlaff, D. (2015). Stream water age distributions
1290 controlled by storage dynamics and nonlinear hydrologic connectivity: Modeling with high-resolution
1291 isotope data. *Water Resources Research*, 51(9). <https://doi.org/10.1002/2015WR017888>
- 1292 Sprenger, M., Tetzlaff, D., & Soulsby, C. (2017). Soil water stable isotopes reveal evaporation dynamics at the
1293 soil-plant-atmosphere interface of the critical zone. *Hydrology and Earth System Sciences*, 21(7).
1294 <https://doi.org/10.5194/hess-21-3839-2017>
- 1295 Sterling, S. M., Ducharme, A., & Polcher, J. (2013). The impact of global land-cover change on the terrestrial
1296 water cycle. *Nature Climate Change*, 3(4). <https://doi.org/10.1038/nclimate1690>
- 1297 Stevenson, J. L., Birkel, C., Comte, J. C., Tetzlaff, D., Marx, C., Neill, A., Maneta, M., Boll, J., & Soulsby, C.
1298 (2023). Quantifying heterogeneity in ecohydrological partitioning in urban green spaces through the
1299 integration of empirical and modelling approaches. *Environmental Monitoring and Assessment*, 195(4).
1300 <https://doi.org/10.1007/s10661-023-11055-6>
- 1301 Tague, C. L., & Band, L. E. (2004). RHESSys: Regional Hydro-Ecologic Simulation System—An Object-
1302 Oriented Approach to Spatially Distributed Modeling of Carbon, Water, and Nutrient Cycling. *Earth
1303 Interactions*, 8(19). [https://doi.org/10.1175/1087-3562\(2004\)8<1:rrhss>2.0.co;2](https://doi.org/10.1175/1087-3562(2004)8<1:rrhss>2.0.co;2)
- 1304 Tetzlaff, D., Carey, S. K., McNamara, J. P., Laudon, H., & Soulsby, C. (2017). The essential value of long-term
1305 experimental data for hydrology and water management. In *Water Resources Research* (Vol. 53, Number
1306 4, pp. 2598–2604). Blackwell Publishing Ltd. <https://doi.org/10.1002/2017WR020838>
- 1307 Tetzlaff, D., Laudon, H., Luo, S., & Soulsby, C. (2024). Ecohydrological resilience and the landscape water
1308 storage continuum in droughts. *Nature Water*, 2(10), 915–918. [y](https://doi.org/10.1038/s44221-024-00300-
1309 y)
- 1310 te Wierik, S. A., Cammeraat, E. L. H., Gupta, J., & Artzy-Randrup, Y. A. (2021). Reviewing the Impact of Land
1311 Use and Land-Use Change on Moisture Recycling and Precipitation Patterns. In *Water Resources Research*
1312 (Vol. 57, Number 7). <https://doi.org/10.1029/2020WR029234>
- 1313 Trenberth, K. E. (2011). Changes in precipitation with climate change. *Climate Research*, 47(1–2), 123–138.
1314 <https://doi.org/10.3354/cr00953>
- 1315 van Huijgevoort, M. H. J., Tetzlaff, D., Sutanudjaja, E. H., & Soulsby, C. (2016). Using high resolution tracer
1316 data to constrain water storage, flux and age estimates in a spatially distributed rainfall-runoff model.
1317 *Hydrological Processes*, 30(25), 4761–4778. <https://doi.org/10.1002/hyp.10902>
- 1318 Wang-Erlandsson, L., Van Der Ent, R. J., Gordon, L. J., & Savenije, H. H. G. (2014). Contrasting roles of
1319 interception and transpiration in the hydrological cycle - Part 1: Temporal characteristics over land. *Earth
1320 System Dynamics*, 5(2). <https://doi.org/10.5194/esd-5-441-2014>
- 1321 Wu, S., Tetzlaff, D., Beven, K., & Soulsby, C. (2025). DREAM(LoAX): Simultaneous Calibration and Diagnosis
1322 for Tracer-Aided Ecohydrological Models Under the Equifinality Thesis. *Water Resources Research*, 61(3),
1323 e2024WR038779. <https://doi.org/https://doi.org/10.1029/2024WR038779>
- 1324 Wu, S., Tetzlaff, D., Goldhammer, T., & Soulsby, C. (2021). Hydroclimatic variability and riparian wetland
1325 restoration control the hydrology and nutrient fluxes in a lowland agricultural catchment. *Journal of
1326 Hydrology*, 603. <https://doi.org/10.1016/j.jhydrol.2021.126904>

- 1327 Wu, S., Tetzlaff, D., Yang, X., Smith, A., & Soulsby, C. (2023). Integrating Tracers and Soft Data Into Multi-
1328 Criteria Calibration: Implications From Distributed Modeling in a Riparian Wetland. *Water Resources*
1329 *Research*, 59(11). <https://doi.org/10.1029/2023WR035509>
- 1330 Yang, X., Tetzlaff, D., Müller, C., Knöller, K., Borchardt, D., & Soulsby, C. (2023). Upscaling Tracer-Aided
1331 Ecohydrological Modeling to Larger Catchments: Implications for Process Representation and
1332 Heterogeneity in Landscape Organization. *Water Resources Research*, 59(3).
1333 <https://doi.org/10.1029/2022WR033033>
- 1334 Ying, Z., Tetzlaff, D., Comte, J.-C., Wu, S., & Soulsby, C. (2025). Storage Dynamics and Groundwater–Surface
1335 Water Interactions in a Drought Sensitive Lowland Catchment: Process-Based Modelling as a Learning
1336 Tool. *Hydrological Processes*, 39(5), e70141. <https://doi.org/https://doi.org/10.1002/hyp.70141>
- 1337 Yuan, X., Wang, Y., Ji, P., Wu, P., Sheffield, J., & Otkin, J. A. (2023). A global transition to flash droughts under
1338 climate change. *Science*, 380(6641). <https://doi.org/10.1126/science.abn6301>
- 1339 Zhang, L., Dawes, W. R., & Walker, G. R. (2001). Response of mean annual evapotranspiration to vegetation
1340 changes at catchment scale. *Water Resources Research*, 37(3). <https://doi.org/10.1029/2000WR900325>
- 1341